CHARACTERIZATION OF HFAPNB AND PHOST AS A POLYMER SENSING LAYER IN AN INTERFEROMETRIC EVANESCENT-WAVE SENSOR

A Thesis
Presented to
The Academic Faculty

by

Karla Ann Dennis

In Partial Fulfillment
Of the Requirements for the Degree
Master of Engineering in Chemical Engineering

Georgia Institute of Technology
August 2009

CHARACTERIZATION OF HFAPNB AND PHOST AS A POLYMER SENSING LAYER IN AN INTERFEROMETRIC EVANESCENT-WAVE SENSOR

Approved:

Clifford L. Henderson, Chair
School of Chemical and Biomolecular Engineering
Georgia Institute if Technology

Stephen E. Ralph
School of Electrical Engineering
Georgia Institute of Technology

Pete Ludovice
School of Chemical and Biomolecular Engineering
Georgia Institute of Technology

DATE APPROVED: June 18, 2009

ACKNOWLEDGEMENTS

Over the course of the past years, many people have given me their advice, suggestions and encouragement in the project. They not only have contributed this work, but also have had an impact on my life both professionally and personally. For these efforts, I would like to say thank you. All assistance has been greatly appreciated. Especially I would like to thank the following people.

1. Dr. Clifford Henderson:
    a. For introducing me to this project
    b. For challenging me to find solutions and drive for results
    c. For helpful discussions around the polymer sensing material

2. Dr. Jeffery Lillie
    a. For discussing results and problems
    b. For introducing me to new instrument measuring systems
    c. For challenging the results
    d. For working with me on the project at any hour

3. Dr. Mikkel Thomas
    a. For skillfully processing the waveguides, chips and lasers
    b. For continually supporting me to complete this thesis
    c. For working with me on the project at any hour
    d. For always giving me something to smile about

4. Dr. Benita Comeau
    a. For beginning the project with me and helping to understand the concepts
    b. For always supporting me through the rough times

5. A special thanks to those that made this project possible
    a. Dr. Nan-Marie Jokerst—Project Head
    b. Dr. Martin Brooks—CMOS Circuit Design Advisor
    c. Dr. Daeik Kim—CMOS Circuit Design
    d. Dr. Stephen E Ralph--

Last , but not least I would like to thank my husband, Taylor for his unwavering support as I pressed forward in completing this thesis. His constant love and support and extraordinary patience and understanding helped me to fulfill my dream.

TABLE OF CONTENTS

LIST OF TABLES

LIST OF FIGURES

LIST OF ABBREVIATIONS

CMOS – complimentary metal-oxide semiconductor

EWS---Evanescent-Wave Sensor

HFAPNB – bis-trifluoromethylcarbinol substituted poly(norbornene)

IC – integrated circuit

M_w – weight average molecular weight

PAG – photoacid generator

PEB – post exposure bake

PGMEA – propylene glycol methyl ether acetate

PHOST – poly(hydroxystyrene)

QCM – quartz crystal microbalance

SSE – sum squared errors

SCCM - standard cubic centimeter per minute

t-BOC – tert-butyloxycarbonyl

TPS-Nf – triphenylsulfonium perfluoro-1-butanesulfonate

UV - ultraviolet

SUMMARY

With an increased concern for homeland security, the need and desire for us to monitor all aspects of our environment in real time has escalated. Furthermore, more conventional fields, such as pollution control and health and safety monitoring, often require the detection of contaminants and analytes at low concentrations. In may of these applications, due to the desired real-time nature and widely distributed areas of interest to be monitored, point of interest monitoring using compact portable measurement tools and sensors is required. Because of this desire, there has been an enormous amount of energy and resources put into developing sensors for many applications. Biological and chemical sensors can provide information critical to health, safety, environmental quality, medical testing, and efficiency, yet many are bulky, slow and expensive to purchase, deploy, and interrogate. Moving forward, sensors in these areas must be made small, portable, robust, rapid, and low power. The central objective of this research is to fulfill this need with the development of a fully integrated on-chip, optical, interferometric sensor that interacts with chemical or biological agents that are present in a gaseous environment. The focus of this research has been the design and fabrication of these interferometric sensors integrated in three dimensions on a chip platform directly on top of a Si CMOS VLSI detector, laser source, and signal processing circuitry. A critical element in the early states of this work was, the selection of a suitable sensing layer material and method for applying it to the interferometric waveguide sensor devices. This project has been a group effort, with collaboration between four groups, three

electrical engineering groups and one chemical engineering group. A more detailed analysis of each contribution will be discussed later.

CHAPTER 1

Introduction to different types of sensors and their applications

1.1 Introduction

A chemical sensor is a device which responds to a particular analyte in a selective way through a chemical reaction and can be used for the qualitative or quantitative determination of the analyte[1]. Chemical sensors can be broken down into two parts, the selective region where the chemistry takes place and the transducer. A transducer responds to a signal such as a color change, emission of fluorescent light, electrical potential change at the surface, an oscillator frequency change of a crystal and many others[2]. There are four main types of transducers for chemical sensors; electrochemical, gravimetric (mass sensitive), thermal and optical. In order to understand the context of the overarching sensor development project that emcompasses the work described in this thesis and to better understand and compare the capabilities of the developed sensor platform and materials, a brief description of these sensor types is provided here.

1.2 Electrochemical Sensors

There are four main types of electrochemical transducers: Potentiometric, Voltammetric, Conductometric, and Field Effect Transistors (FET). All involve the measurement of a potential or electrical current, and indirectly a material's conductivity. A potential can be described by having a charge separation across the boundary, for example between a metal and the solution.

1.2.1 Potentiometric Sensors

Potentiometric sensors measure a cell potential at zero current. One classic example of a potentiometric sensor is the ion selective electrode. The key element of the ion selective electrode is a porous hydrophobic membrane, made of either a liquid membrane or a thin polymer membrane which is in contact with an organic liquid as shown in Figure 1.1.

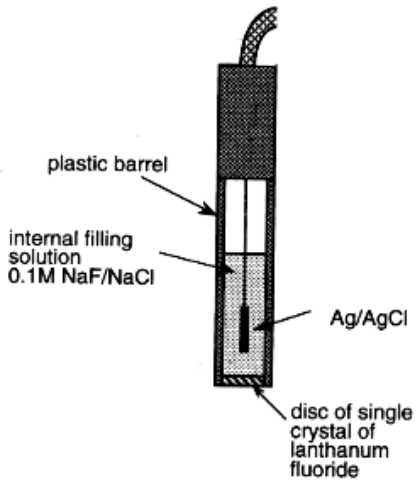

Figure 1.1: The Fluoride Ion Selective Electrode is a type of potentiometric sensor which exchanges ions with the solution sample

In the device shown in Fig. 1.1, the crystal of lanthanum fluoride acts as the ion-selective membrane which exchanges with ions in the sample solution. Depending on the choice of organic liquid, the electrode can be sensitive for different ions. The potential of the electrode is measured against an appropriate reference electrode. The sensor operates like that of a concentration cell, it develops a potential across the membrane between the sample solution and the reference. These sensors have been used for sensing calcium for the hardness of water, potassium and sodium in biological fluids, and many others.

1.2.2 Voltammetric Sensors

Voltammetric sensors are different from potentiometric sensors. These measure the current flowing in the cell as a function of the applied material[1]. The amount of current that a cell produces is directly related to the concentration of the cell. This can be traced back to the species undergoing an oxidation or reduction. Two successful voltammetric sensors are the oxygen probe, more commonly referred to as the Clark electrode, and the glucose biosensor. The Clark electrode is used to determine the dissolved oxygen concentration in solutions, and is particularly common in the testing oxygen levels in water during environmental studies[2]. The voltammetric glucose sensor is now a commonplace item in home healthcare and is a must for individuals monitoring their diabetes. Figure 2 shows an example of a Clark electrode.

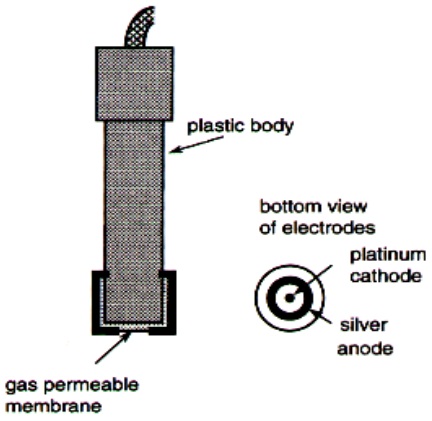

Figure 1.2: The Clark Electrode is a type of voltammetric sensor used in environmental studies for dissolved oxygen

1.2.3 Conductivity Sensors

Conductivity sensors measure the ease of passage of electric currents through a solution. This relationship is governed by Ohm's law.

$$E=IR \qquad [1.1]$$

E= potential difference across the resistance
I= Current
R= Resistance

Conductivity is directly related to the concentration of ions in the solution. The conductivity of the cell varies with the charge on the ion, the ion mobility and the dissociation of the ion[2]. With all these factors affecting the conductivity of the cell, it has no selectivity and therefore can only be used in controlled situations.

1.2.4 Field Effect Transistors

Field-effect transistors(FETs) are devices in which a transistor amplifier is adapted to be a miniature transducer for the detection and measurement of potentiometric signals[2]. But one of the major disadvantages of these is that they require a reference electrode. Because of the problem of miniaturizing the reference electrode no suitable small FET sensor exists. Figure 3 shows a schematic of a field-effect transistor with a chemically sensing gate surface. In this arrangement the chemically sensitive membrane is in contact with the analyte solution.

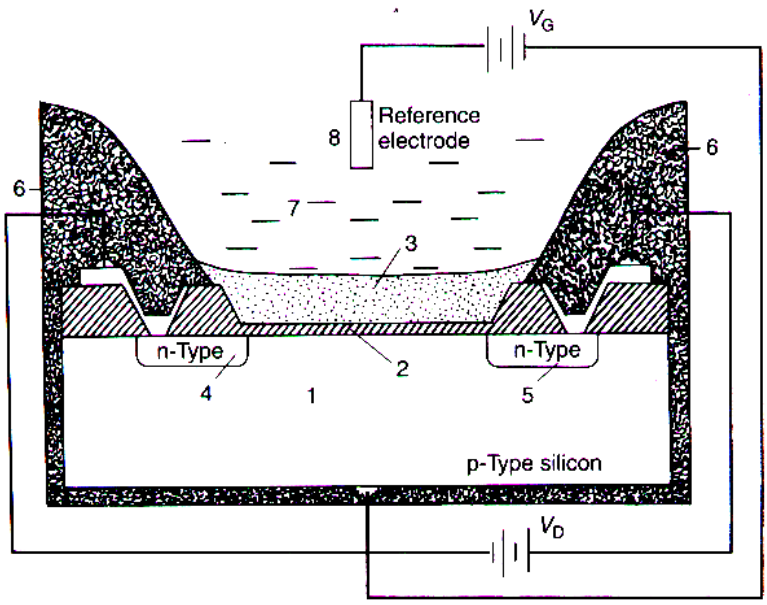

Figure 1.3: Field Effect Transistors where 1. silicon substrate, 2. insulator, 3. chemically sensitive membrane, 4. source, 5. drain, 6. insulating encapsulant; 7. analyte solution; 8. reference electrode.

1.3 Gravimetric Sensors - Mass Sensitive Devices

1.3.1 Surface Acoustic Wave Sensors (SAW) Introduction

One general type of mass sensitive sensors in very common use is the surface acoustic wave (SAW) sensor. It uses the concept of the piezo-electric effect. When a chemical reaction has taken place there is normally a change in mass. This change in mass can be detected if a very sensitive microbalance is used. The piezo-electric effect is basically a conversion of mechanical to electrical energy. When stress such as pressure is applied to crystals such as quartz, which does not have a center of symmetry, the crystal lattice is deformed and an electrical potential is developed[3, 4].

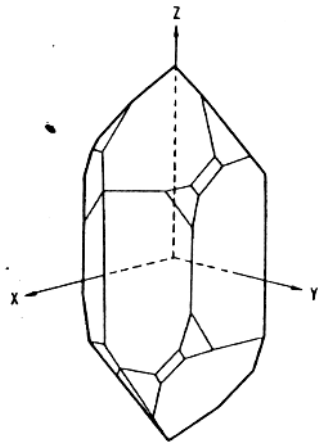

Figure 1.4: Three different axes for a quartz crystal, a) longitudinal b) lateral c)torsional

A current will flow in an external circuit if electrodes are connected to the crystal. This alternating potential difference to the crystal causes mechanical oscillations at a natural resonant frequency. When these forces are induced it can cause the crystal to vibrate in 3 different directions; longitudinal (extensional), lateral (flexural and shear), and torsional (twist). Figure 1.4 above shows the three different axes of a quartz crystal. This resonant frequency will change if material is deposited on the surface or if the physical dimensions of the crystal change. Shown below is an example of what a finished quartz crystal looks like.

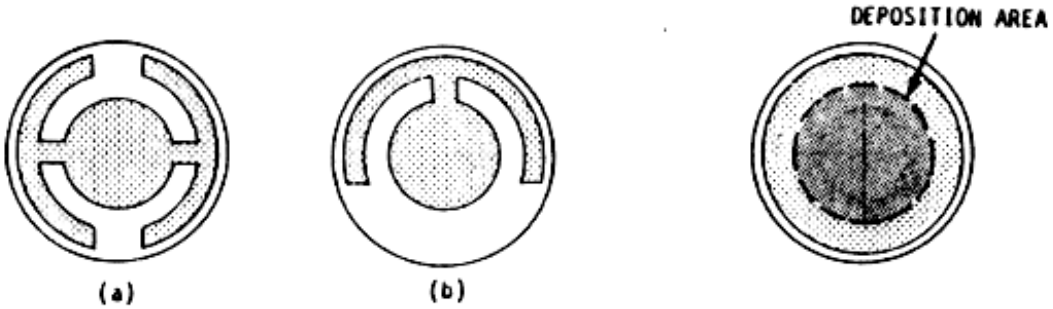

Figure 1.5: The quartz crystal in it's finished state. Caption a and b shows two examples of the back patterns of the crystal with gold electrodes and the far right shows the deposition area.

1.3.2 Types of Surface Acoustic Wave Sensors (SAW)

These sensors are formed using piezo-electric crystals. Instead of having the waves be generated in the bulk of a solution, the waves are generated on the surface of the SAW sensors. As shown in Figure 1.6 there is a transmitter and a receiver positioned on opposite ends of the sensor. At both the transmitter and the receiver are sets of interdigitated electrodes.

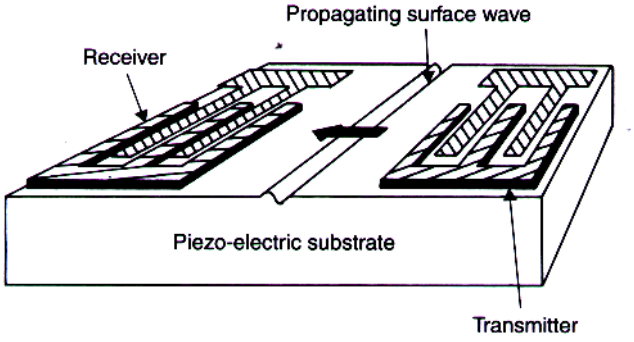

Figure 1.6: Surface Acoustic Wave Sensor with interdigitated electrodes at the transmitter and receiver ends

A mechanical stress that is caused by a radiofrequency signal produces a Raleigh-type surface acoustic wave; it then propagates along the surface where the second set of interdigitated electrodes receives and translates it to an electrode voltage. There are four main types of SAW's: plate mode, evanescent wave mode, lamb mode and thickness shear mode.

1.4 Heat sensitive

Heat sensors are more commonly called calorimetric sensors. When a chemical reaction takes place it is either exothermic or endothermic. Monitoring this heat with a transducer such as a thermistor or platinum thermometer has been a source for valuable sensors. There are three basic classes of calorimetric sensors, the temperature probe, catalytic sensors, and thermal conductivity.

1.4.1Temperature Probe

A thermistor involves the measurement of heat of a reaction on its surface. The change in temperature is based on a decrease in electrical resistance. There are two approaches in the use of a temperature probe, the thermistor can be integrated in the detector cell to measure the temperature change after the analyte solution has passed through an immobilized enzyme bed or the enzyme can be attached to the surface of the thermistor itself. Two examples of themistors that have been successful in this type of calorimetric sensing, the glucose and urea calorimetric sensors. Figure 1.7 shows a calorimetric enzyme-coated sensor which can be tailored for either glucose or urea.

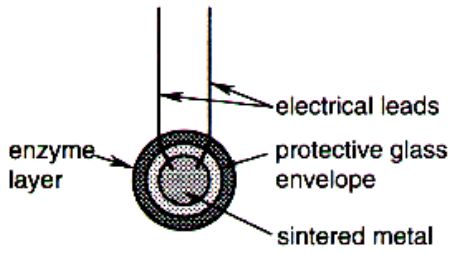

Figure 1.7: Calorimetric enzyme-coated sensor, which can be used for either glucose or urea depending on the enzyme layer

1.4.2 Catalytic Sensors

Catalytic sensors are used in the detection of flammable gases and vapors in the air. Since these gases are extremely volatile, a rapid response is needed and therefore a catalyst is used. This sensor uses a heater to keep the sensor at a constant temperature to combust the gas. A coil of wire is the heater. The combustion of gas occurs at the surface and causes an increase in temperature. This increase in temperature is related to the amount of gas combusted. The most well known catalytic sensor is the pellistor. The pellistor is shown in Figure 1.8

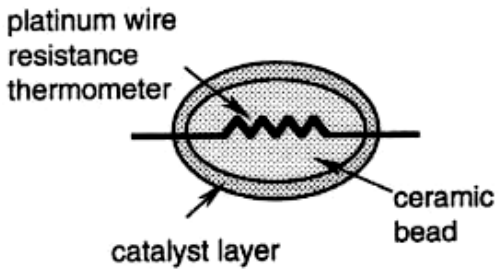

Figure 1.8: An example of a catalytic sensor known as the pellistor.

The pellistor uses a platinum coil as the heater and palladium as the catalyst. The coil acts as both a heater and as a resistance thermometer. The temperature of the pellet and the coil increases as heat is released from a combustible gas reacting at the catalytic surface. This increase in temperature increases its resistance.

1.4.3 Thermal conductivity

Thermal conductivity sensors are used when the detection of high concentration of gases is needed. Compared to the other two heat sensitive sensors, thermal conductivity sensors do not require a chemical reaction to take place on the sensor surface; instead it uses the thermal conductivity of the gas. This sensor involves heating a filament, usually of tungsten. Heat is lost from the filament to the surrounding area. This heat loss is dependant upon the thermal conductivity of the surrounding gas. Therefore as the temperature changes in the filament a concentration of gas can be detected. An example of this type of sensor is the gas chromatography which is shown in Figure 1.9. There are many detectors which can be used in gas chromatography. Different detectors will give different types of selectivity. A *non-selective* detector responds to all compounds except the carrier gas, a *selective detector* responds to a range of compounds with a common physical or chemical property and a *specific detector* responds to a single chemical compound. Detectors can also be grouped into *concentration dependant detectors* and *mass flow dependant detectors*.

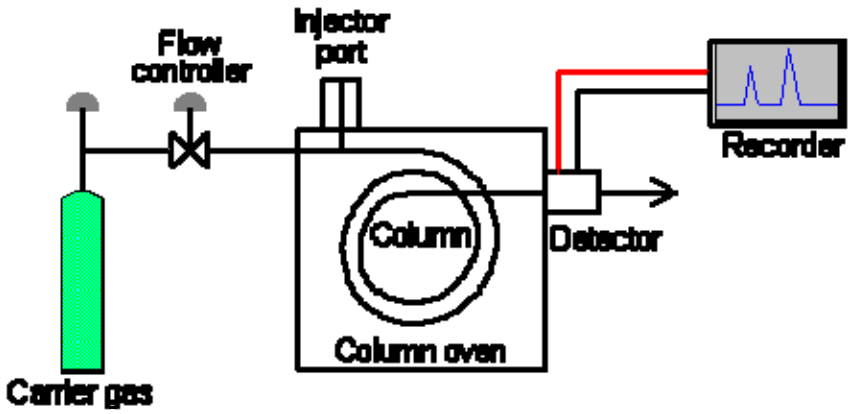

Figure 1.9: Generic schematic of a gas chromatography. Detector can be a non-selective, selective, specific detector, concentration dependent, or mass flow detectors.

1.5 Optical Sensors

Fiber optic sensing has opened a broad area for scientist in the analytical world. They serve in major fields such as medical and chemical analysis, molecular biotechnology, marine and environmental analysis, industrial production monitoring and bioprocess control, and the automotive industry[5-7]. Optical sensors have been developed for pH sensing, metal ion sensing, glucose and penicillin biosensing, oxygen sensing and many more. They are able to perform in areas that are inaccessible for other spectroscopy sensing, yet they still offer a wide spectral range.

Fiber optic sensing is based on either an indirect or direct method of detection. For indirect sensing the color or fluorescence of an immobilized indicator, label or any other optically detectable bioprobe is monitored. For the direct method, properties of the analyte are measured, such as refractive index, absorption or emission[7]. There is a broad range of optical sensors.

Absorbance, reflectance, luminescence, and index-based optical sensors can be associated with a chemical reaction. These are the four main techniques for optical sensing.

The simplest type of optical sensor uses absorbance. It measures the percent reduction in light that passes through a solution to be analyzed. Absorbance can be used to monitor methane gas in coal mines and radioactive elements such as uranium and plutonium in nuclear processing. In some applications, it is necessary to react the analyte with a reagent. Then it is necessary to immobilize the reagents in a film or bind them to a substrate. Light is transmitted through an optical fiber in contact with the membrane and

then the transmitted light is collected by a second fiber[1]. This type of optical sensor is shown in Figure 1.10.

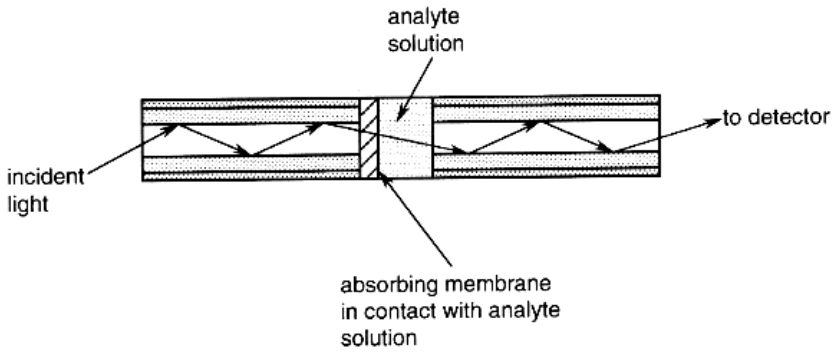

Figure 1.10: Optical Sensor configuration for absorbance measurements where light is transmitted through a fiber in contact with the absorbing membrane.

Second, reflectance measurements are necessary when the membrane or medium being used will not allow light to be transmitted through it. Instead of having a second fiber to collect the data after the analyte has reacted with the film, the light is reflected. This reflection will determine the concentration of the analyte. Shown below in Figure 1.11 is the configuration for reflectance measurements in optical sensing.

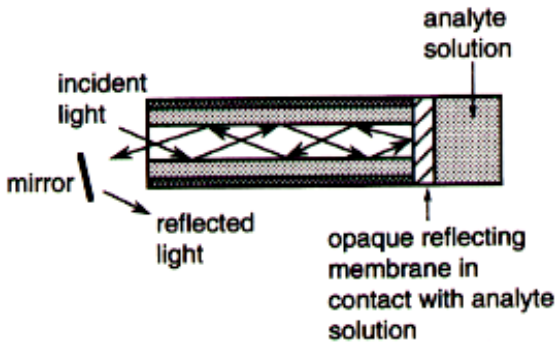

Figure 1.11: Optical Sensor configuration for reflectance measurements. Light is propagated through and reflected off the membrane.

Last, luminescence measurements are connected with the emission of radiation. Two examples of luminescence are fluorescence and phosphorescence. In biochemical sensing, fluorescence measurements are sensitive and selective which allows low concentration of an analyte to be determined. This absorption of light that leads to fluorescence follows the Beer-Lambert Law and can be directly related to the amount of absorbed radiation and to the concentration of analyte[1].

$$I_f = 2.303 * \phi_f * I_o * \varepsilon * b * [M] \qquad [1.2]$$

Φ = quantum efficiency
I_o = initial light intensity
ε = molar absortivity
b = path length of sample
[M] = concentration of the compound

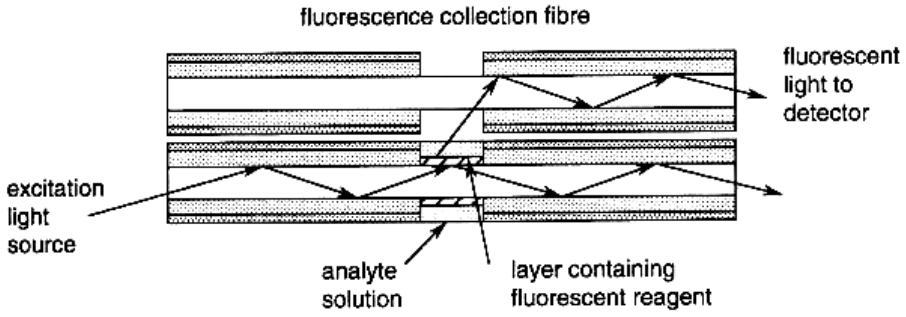

Figure 1.12: Optical Sensor configuration for fluorescence and evanescent transmission

Some examples of optical sensing are listed below. Because the substrate of the sensor being constructed is a semiconductor, the discussion will be tailored to examples of sensors in this area.

1.5.1 Chemical and Biological Sensing

One major area for chemical and biological sensing is to use a Mach-Zehnder interferometer (Fig. 1.13.) The Mach-Zehnder interferometer is first a waveguide which guides electromagnetic radiation by total internal reflection. Light emitted from the embedded laser is split in the y-junction. It then passes through two parallel waveguides. One of these is a reference waveguide which is insensitive to chemical agent. The other arm is an analyte waveguide portion. The electromagnetic radiation is then converged in the second y-junction into an exit beam. The external surface of at least the analyte portion is covalently modified, or functionalized, relative to the reference portion. The resulting interaction of the functionalized surface with molecules comprising an analyte causes a phase change in the electromagnetic radiation passing through the analyte

portion relative to the reference portion. This generates a corresponding and measurable interference pattern in the exit beam[8-11]."

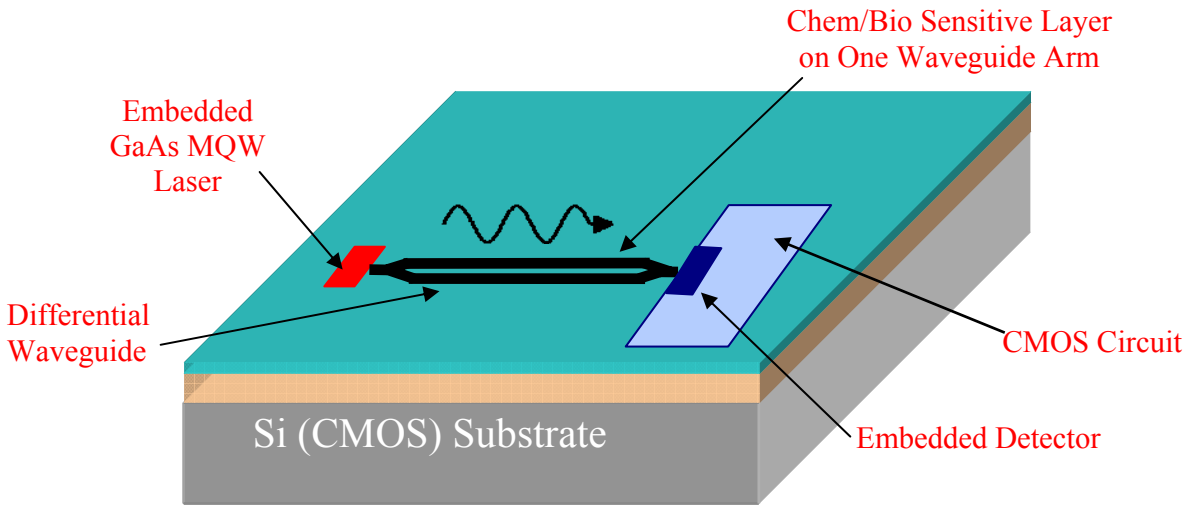

Figure 1.13: Picture of a Mach Zehnder Interferometer that is fully integrated with an embedded laser and detector on a silicon substrate.

The surface of the substrate can be glass, plastic, a crystal or a semiconductor. These systems have the ability to combine numerous types of components on a single substrate which produces a wide band of functionality. There are two different options for accomplishing this task; either by integrating the lasers, waveguides, and photodetectors or by using multiple interferometers to detect different analytes.

1.5.2 Environmental Sensing

A Mach-Zehnder waveguide sensor has been used for detection of agricultural contaminants such as atrazine, which is a herbicide[8]. One attractive aspect of this sensor is that it is able to monitor continuously and have a sample analyzed within 10 minutes, while traditional analyzing techniques such as high-performance liquid chromatography, and gas chromatography with mass spectroscopy requires pretreatment and preconcentration which makes these very time consuming.

1.5.3 Chemical Sensing

It has also been shown that a Mach-Zehnder interferometer can be functionalized with a covalently bound intermediate gold layer on the surface for sensing applications[12]. The specific binding of streptavidin desthiobiotin as well as an antibody was demonstrated. This sensor however still needs to be optimized to achieve the required sensitivity.

1.5.4 Pressure Sensing

The Mach-Zehnder interferometer is also used for pressure measurements. There are two channels or arms, one arm of each interferometer traverses a diaphragm etched from the wafer backside. On the active arm or channel of the waveguide three diaphragms were integrated, the other had no diaphragms and was used as a reference. The core that was selected for sensing was oxynitride. Any deflection of the diaphragms caused changes in the core. In Figure 1.14 shows the schematic of the pressure sensor. This waveguide technology is based on anti-resonant reflecting optical waveguides (ARROW)[13].

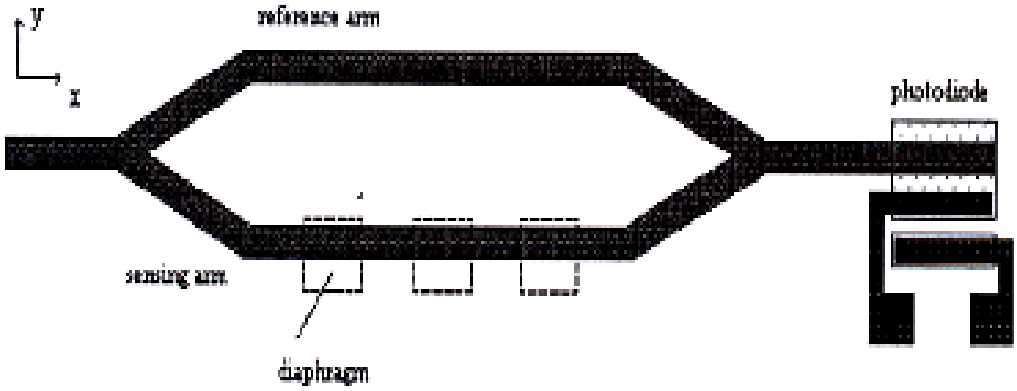

Figure 1.14 Interferometric Pressure Sensor schematic

1.5.5 Displacement Sensors

Displacement Sensors uses light to perform measurements of an object's movement. As shown in Figure 1.15 a Michelson interferometer is used.

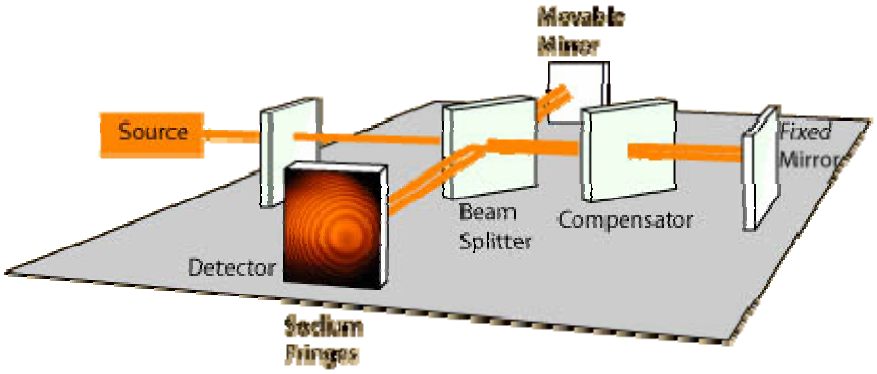

Figure 1.15 Schematic of a Michelson Interferometer

A mirror divides the optical field into a measurement and reference arm. Reflection from a moving external object causes a phase shift with respect to the reflection from the fixed mirror in the reference arm[13]. Once the reflected beams are brought back together, an interference pattern results.

1.5.6 Other optical Sensors

Other examples of optical sensing besides interferometry are holography and surface plasmon resonance. Surface plasmon resonance (SPR) has a specific geometry that allows the surface plasmons to interact with the analyte on the opposite side of the metal film, usually gold. SPR arises when light is reflected from a conducting film at the interface between two media of different refractive index. The SPR depends on three experimental variables, the incident beam angle, the incident beam wavelength and the refractive index near the surface where plasmons propagate[14]. Molecules in the sample can bind to the surface. Once bound, these molecules are the cause of a refractive index change at the surface and the SPR responds. Shown in Figure 1.16 is an example of an SPR and a response curve of the minimum reflected light.

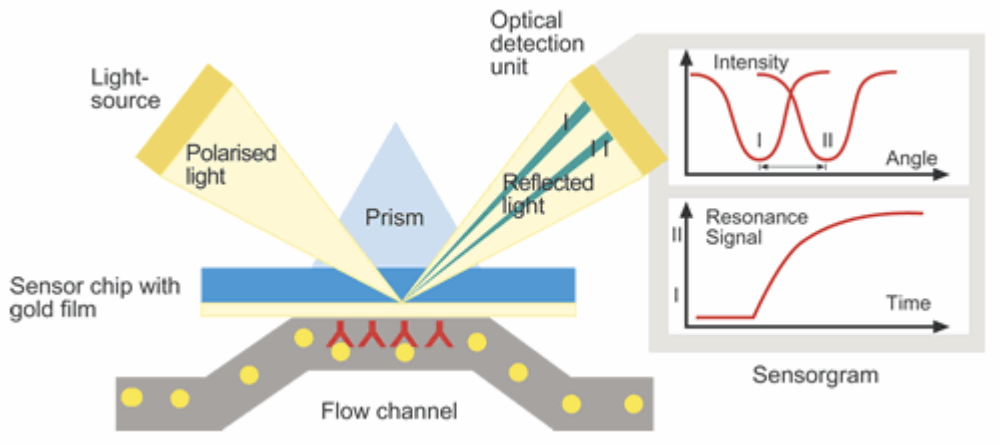

Figure 1.16: Surface Plasmon Resonance and a typical response curve

Our design of an integrated mach-zehnder interferometric sensor has been based on the Hartman biosensor. Some of the key components of the Hartman sensor includes separate sensing and reference waveguide arms, an IO interferometer chip, diode laser, and a photodiode detector[15-17]. The Hartman biosensor shown in Figure 1.17 detects the change in effective index created by the sensed agent.

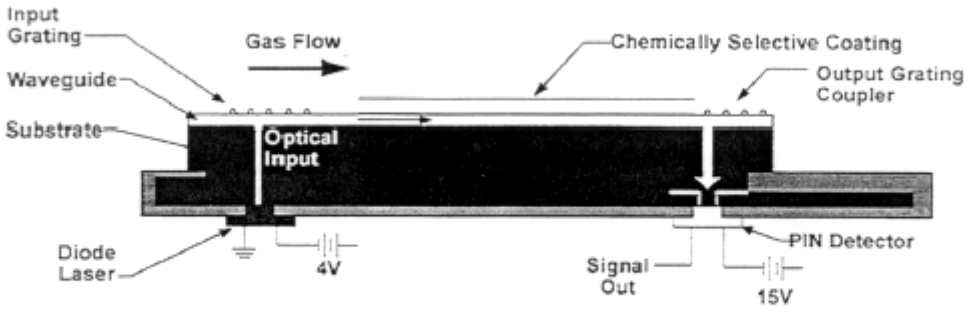

Figure 1.17: Cross sectional view of the Hartman Interferometric Biosensor

As light propagates under the sensing region, a change in the phase shift is experienced by the modes of the waveguide. This light from the laser can either be a single mode or multi mode. This laser light couples into the multimode waveguide creating a multimode pattern. Regardless of the source, some points in the pattern will increase in intensity and others will decrease, which is an indication of a chemical detection. The top view of the Hartman interferometric sensor is shown in Figure 1.18. The biological sensing layer is exposed to the environment. The optical wave, which is generated by a beam combining/splitting element travels down the two arms. The

interference that is generated is used to calculate the change in refractive index. The Hartman sensor has detected different analytes such as benzene, xylene, toluene and chloroform at less than 1 ppm[15].

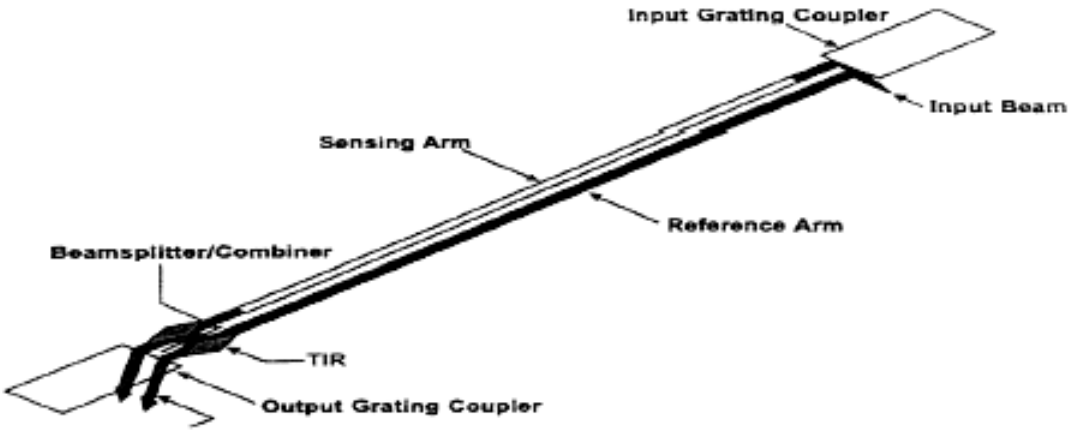

Figure 1.18: Top view of the Hartman Interferometric Biosensor

CHAPTER 2

The Project Scope

2.1 Fabrication and Characterization of Interferometric Sensor

As stated before this project was a collaboration of different groups, the major objective of the research was the fabrication and characterization of an optically embedded interferometric sensor on standard Si CMOS circuitry, shown in Figure 2.1.

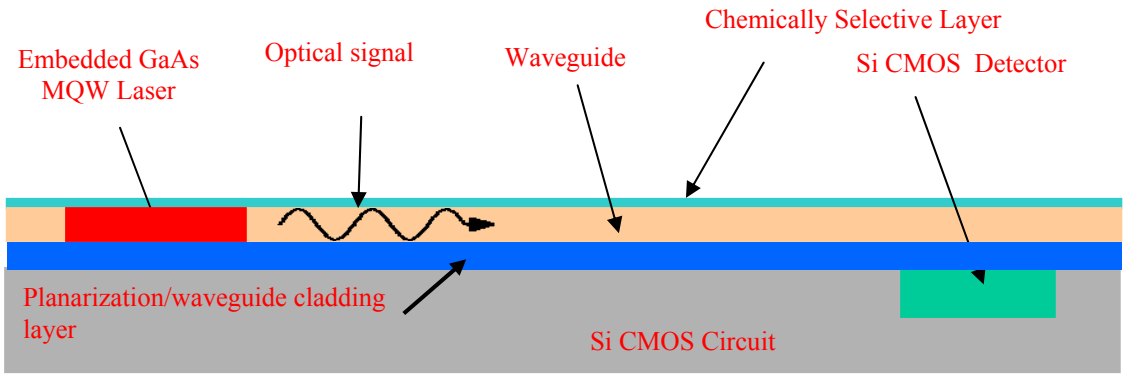

Figure 2.1 Optically embedded interferometric sensor on standard Si CMOS circuitry.

Four major areas of this sensor are the chip and detector arrays, the thin film laser source, the interferometer waveguide and the chemically sensitive polymer.

2.1.2 Detector Arrays

The chips photodetectors need to have small dimensions to resolve the intensity pattern emitted from the sensor. They must detect small changes in intensity and exhibit minimal noise. The on-chip photodetectors are an 8umx8um in size. Signal processing

of the detected interferometer pattern is performed by on-board analog-to-digital converters on the CMOS circuit. Not only the detectors, but also the converters and the circuitry must exhibit the same low noise and high sensitivity. This work is being completed by Dae-ik Kim from the Electrical Engineering department at Georgia Institute of Technology.

2.1.3 The Embedded Laser

Another major area of interest is the embedded laser. The embedded sensor will consist of an optical emitter launched directly into a SiO_2/Si_3N_4 interferometer. Signal detection will be handled by CMOS detectors fabricated as part of the circuit. The embedded optical emitter will consist of a thin-film edge-emitting laser. A modular approach designed by Mikkel Thomas was used to build the final integration sequence for the sensor: 1. Development of the thin-film edge-emitting laser; 2. Development of the waveguiding structures; 3. Development of thin-film laser embedded in a waveguide; 4. Integration of waveguide structure and embedded sensor on the Si CMOS. One critical element of sensor function is the accurate deposition of both the lasers and the waveguide. This work is being completed by Mikkel Thomas of the Georgia Tech Electrical Engineering Department.

2.1.4 Interferometric waveguide

The waveguide is a Mach-Zehnder interferometer, where one arm has a chemically sensitive polymer. The effective index shift on this arm of the interferometer is detected as a shift in the horizontal multimode pattern at the output facet of the sensor. This output is coupled to the CMOS detectors which capture the multimode pattern, and

then are read out by circuitry. The changes in the multimode pattern are measured and processed to create a large signal in response to chemical absorption in the chemically sensitive polymer. This work is being completed by Jeff Lillie also in the Electrical Engineering department at Georgia Tech.

2.1.5 Chemically Sensitive Polymer Layer

The sensing layer is a crucial aspect to the design. It must exhibit properties that are compatible for standard semiconductor processing and be able to guide light down the length of the waveguide arm. It also has to be able to have a sensitive response to different contaminants that are in the environment, and be able to distinguish between them. This work is discussed in detail as part of this thesis.

2.1.6 The Design

The complete design of the fully integrated, optical evanescent wave sensor is shown in Figure 2.2. It shows all four key aspects discussed above, plus the analog to digital converters.

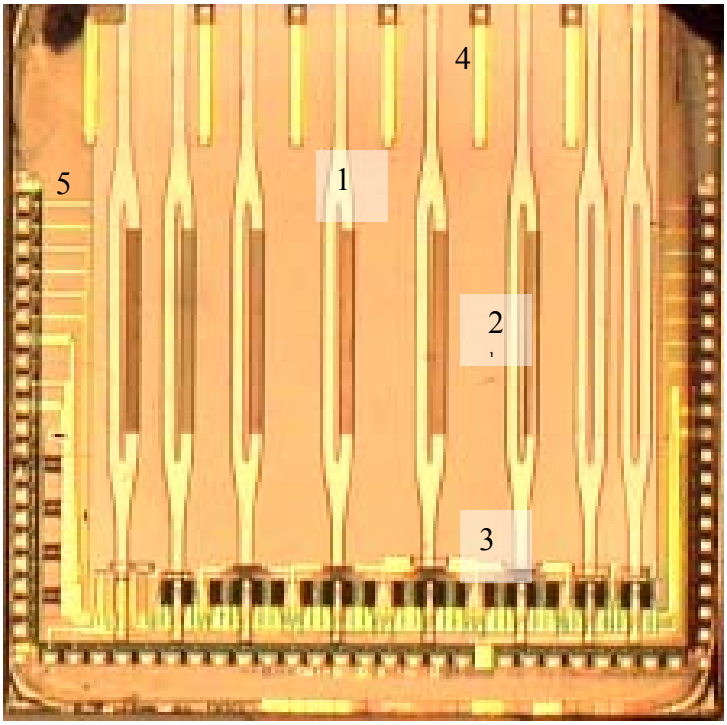

Figure 2.2: Picture of a fully integrated optical sensor where 1: interferometer 2: polymer sensing layer 3: detector arrays 4: location of embedded laser 5: analog to digital conversion points

The cross sectional view for the multimode, Mach-Zehnder, interferometric sensor is shown in Figure 2.3. The interferometer has been fabricated on silicon. The device is 4500-um long and has 100-um wide waveguides. On one interferometer arm, there is a 2000-um long, 100-um wide sensing region.

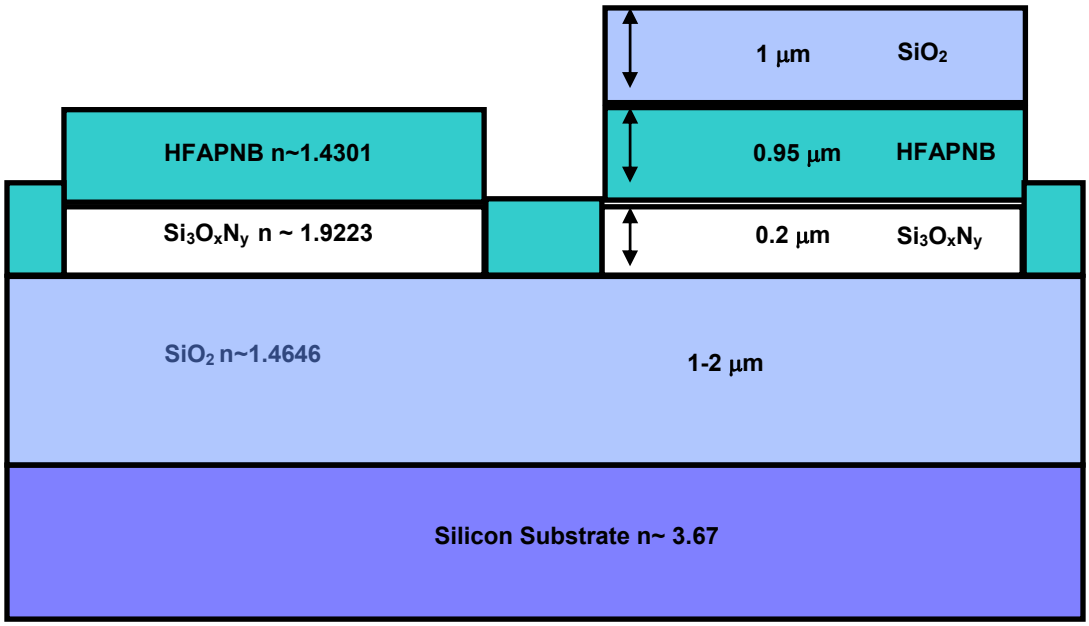

Figure 2.3: The layer structure at the central cross section of the interferometric EWS which includes on the top a chemically sensitive polymer, HFAPNB or PHOST.

The structure above the silicon includes a 1-um SiO_2 buffer layer (n632.8nm~1.477); a 0.25-um, high index(n632.8nm~1.921), low loss, silicon oxynitride(SiO_xN_y) guiding layer, and a 1-um SiO2 buffer overlayer. On one interferometer arm, a 2000-um2, etched channel is filled with a 1-um thick layer of the sensing polymer, hexaflouroisopropanol-substituted polynorbornene, HFAPNB(n632.8nm~1.451). As stated before the sensor operates by detecting changes in the index of refraction of the waveguide. The optical fields that propagate down the waveguide have an evanescent field that penetrates into the region above the waveguide core. This upper region contains the chemically selective polymer. If more of the light extends into the polymer layer, the optical pulse becomes more sensitive to any change in

the polymer refractive index. These index changes alter the phase of the propagating wave. These phase changes are easily detected by mixing or interfering the shifted pulse in the sensing arm with that of the reference arm. An example of the light propagating through a waveguide and extending into the sensing layer is shown in Fig. 2.4. It should be noted that this figure is singlemode vertically and multimode in the transverse direction.

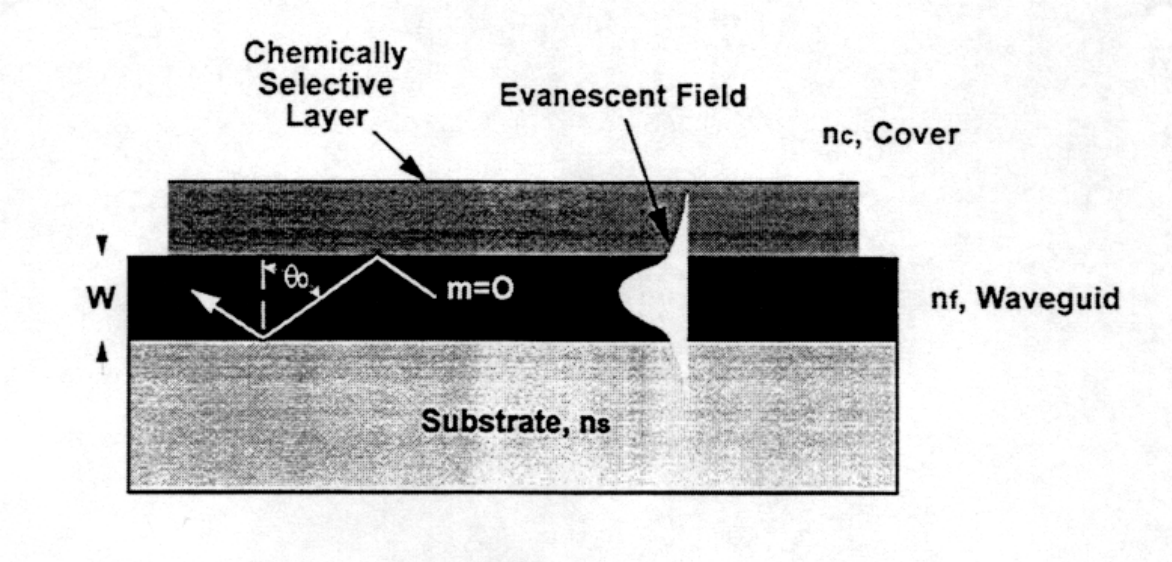

Figure 2.4 Side profile of an optical waveguide showing a large evanescent field passing through the chemical sensing layer

2.1.7 Design Setup

A gas delivery system was constructed to supply the test chamber with a chemical environment. A vertically polarized, 632-nm Helium-Neon laser is focused by a microscope objective and couples to the interferometer, which is positioned in the test chamber. The output from the test chamber then is directed through another microscope objective which images the multimode intensity profile to a linear CCD array. Modal

patterns at the output are normalized by total power and recorded at regular time intervals to track pattern changes. After the chemical environment that is supplied to the test chamber which holds the waveguide, it also passes through a quartz crystal microbalance (QCM) chamber. By matching these measurements, modal pattern changes and the QCM measurements with the ellipsometry-based simulations, a link between sensor response and index changes within the sensing layer is established. This correlation between the two responses is discussed in further detail later. The experimental design setup is shown in Fig. 2.5.

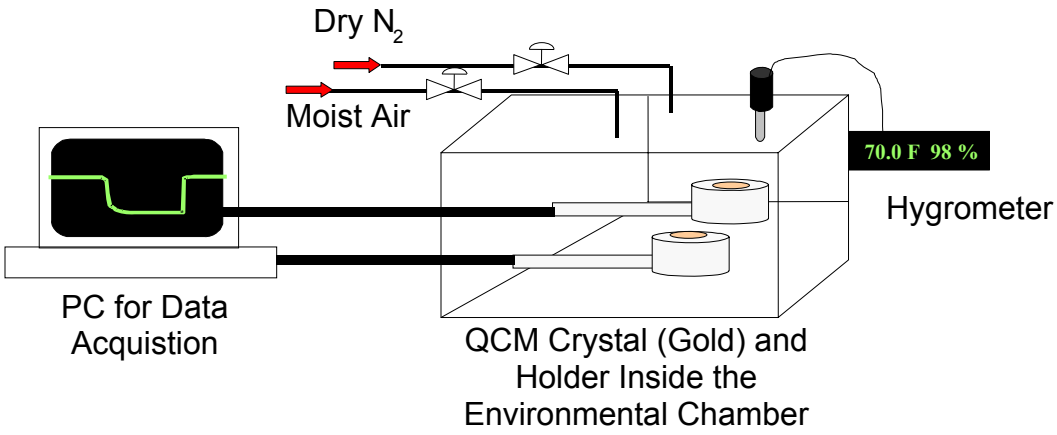

Figure 2.5: Basic experimental setup used for QCM water sorption experiments. Only one of the two QCM holders is shown.

CHAPTER 3

Polymeric Sensing Layer Materials

3.1 Introduction to Sensing Layers

The sensing layer is one of the most important aspects to designing a waveguide. Some of the characteristics that the sensing layer must be comprised of is it must change in response to the analyte. This is critical to the selection and sensitivity. It must also exhibit high optical transparency at the wavelengths of interest. The transmission was measured at 840 nm of greater than 93% for this particular work. The sensing layer has uses for both non-reversible and reversible chemical absorption when exposed to different hydrocarbons. It also needs to be somewhat temperature resistant so that the refractive index does not change due to this variable.

In this work, since CMOS structures were prefabricated on Si, it was desireable to develop a CMOS compatible process for depositing the sensing layer materials on the waveguides. It was desided that the easiest method would be to spin coat and photo pattern the polymers. This process could be further simplified if the sensor polymers themselves could be made directly photodefinable. Therefore, polymers used as photresist resins where considered. If the polymer is used as a core material it must have a refractive index higher than that of the cladding polymer[18-20]. However, currently this polymer is used as a chemically sensitive cladding. The thin (0.2 micron) high-index silicon oxynitride core (n840nanometers ~ 1.92) of the waveguide forces a large fraction of the light into this chemically sensitive polymer, creating the sensing. Two such

polymers that meet these criteria have been tested, polyhydroxystyrene (PHOST) and hexafluoroispropanol (HFAPNB).

3.1.2 PHOST

Poly(p-hydroxystyrene) (PHOST, Mw = 11,800) was obtained from DuPont Electronic Materials (formerly Triquest Chemical Company). PHOST is a common polymer used in 248 nm photolithography, and its structure is shown in Figure 3.1. For early testing, sorption of water and simple alcohols were tested as analytes with this material due to the ease of handling and the availability of literature data for validation of results. The abundance of hydroxyl groups in this polymer results in a relatively polar matrix that has an affinity for polar compounds such as water and alcohols.

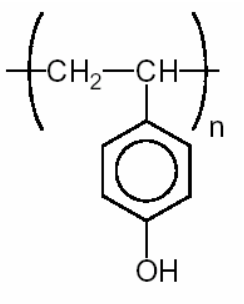

Figure 3.1: PHOST

3.1.3 HFAPNB

Bis-trifluoromethyl carbinol substituted polynorbornene (which is commonly referred to as hexafluoroispropanol substituted polynorbornene or HFAPNB, Mw = 34445) was obtained from Promerus Electronic Materials. HFAPNB is a polymer that belongs to a class of PNB polymers that has been proposed as a polymeric matrix for the development of next generation photoresist materials for 193 nm and 157 nm

lithography. The structure of HFAPNB is shown in Figure 3.2. In this material, the presence of the bis-trifluoromethyl carbinol group provides a strong hydrogen bonding functional group that again provides a strong affinity in this material for polar compounds.

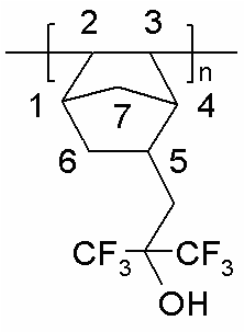

Figure 3.2: HFAPNB monomer

3.2 Preparation of Polymers

Both the PHOST and the HFAPNB are dissolved in propylene glycol methyl ether acetate (PGMEA) (99%) purchased from Aldrich Chemical Company to create a 20 wt% polymer solution. A photoacid generator (PAG), 3 wt% by solids, is added to make the polymers photosensitive to ultraviolet light. This acid increases the solubility of the system. This allows the polymers to be patterned within the waveguide to complete the requirements for the sensor. Figure 3.3 below depicts the outgased products of an 80/20 blocked copolymer HFAPNB and the PAG after they are exposed.

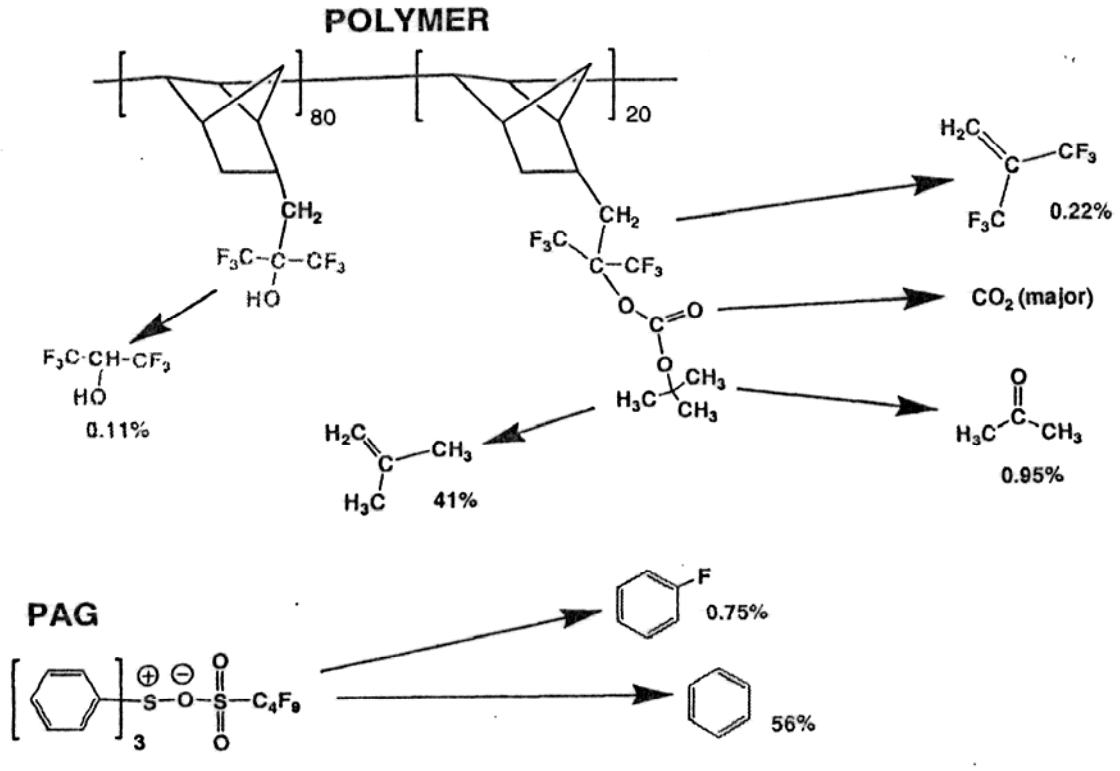

Figure 3.3: Out gassed products of HFAPNB after exposure

3.3 Preparation of Samples

First, the clean silicon wafer is subjected to a primer (only when using HFAPNB), usually hexamethyldisilane (HMDS). This primer improves the adhesion between the photoresist and silicon substrate, through changes in the surface chemistry of the substrate. The primer was spin coated at 5000 rpm for 10 seconds using a CEE Model 100 CB spin coat/bake system to create a monolayer which will allow greater adhesion. Next, the polymer is dispensed through a 0.2 micron Teflon filter to remove particulates and uniformly applied to the surface of the silicon substrate using the spin coater. Because the polymer is photosensitive, it will undergo a chemical change when exposed to ultraviolet light which will create a permanent image in the material. The desired

thickness of the polymer film is around 1 um. This thickness is controlled by the spin speed and time. After spinning, the film is subjected to a 130°C soft bake for one and one half minutes where the majority of residual solvent is removed.

3.4 Calibration of Polymeric Sensor Layer Behavior:

3.4.1 Quartz Crystal Microbalance (QCM) Operational Principle

The total mass of a vibrating body and a few other physical parameters determine the resonant frequencies of a mechanical-vibrational system. In fact, the change in resonant frequencies of a vibrating body is proportional to the amount of material added or removed. The QCM consists of a thin quartz disk with electrodes plated on it, as shown below in Figure 3.4.

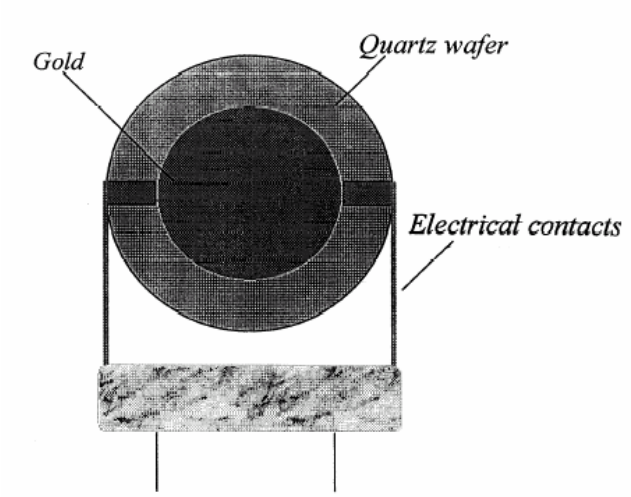

Figure 3.4: Quartz Crystal disk with electrodes plated

Since the QCM is piezoelectric, an oscillating electric field applied across the device induces an acoustic wave that propagates in a direction perpendicular to the crystal surface. A resonant oscillation is achieved by including the crystal into an

oscillation circuit where the electric and mechanical oscillations are near the fundamental frequency of the crystal. The fundamental frequency depends upon the thickness of the wafer, its chemical structure, its shape, the total mass of the crystal, and any rigid films coating the crystal.

The Sauerbrey equation for fundamental resonance (Equation 3.1) gives the relationship between changes in mass per unit area (Δm), and frequency (Δf). This equation assumes that the combination of the crystal and the adsorbed mass behaves together as a rigid assembly.

$$\Delta f = \frac{-2\Delta m f_0^{\,2}}{A\sqrt{\mu_q \rho_q}} \qquad 3.1$$

Where:
A = electrode surface area
μ_q = shear modulus of quartz
ρ_q = density of quartz
f_o = resonant frequency of oscillation

All of the parameters can be lumped into a constant (K), and this relation simplifies to a linear relationship.

$$\Delta f = -C_f \Delta m \qquad 3.2$$

The constant C_f in the system was calculated to be 81,300,000 Hz cm^2/g for a particular frequency of crystals. This relationship allows easy conversion from a change in frequency to a change in mass per area. Then, with a crystal area of 0.5986 cm^2, the total mass uptake is calculated.

3.4.2 Ellipsometry

A sensitive technique that uses polarized light to measure the optical properties of thin films is called ellipsometry. Ellipsometry determines the relative phase change in a beam of reflected polarized light. This measurement is more sensitive than a simple reflection measurement. Also ellipsometry is more accurate than intensity reflectance because the absolute intensity of the reflected light does not have to be measured. Using a J.A Woollam Co Inc Ellipsometer allows ellipsometry to be done at a variety of angle of incidence and wavelengths. By acquiring data over a range of angles of incidence and a range of wavelengths, one is able to uniquely determine optical constants and thickness of a thin film. This allows a very broad range of sample materials and structures that can be used. Also the spectroscopic measurements provide the ability to acquire data in spectral regions where the measured data are most sensitive to the model parameters to be determined.

As stated before the ellipsometer measures the change in polarization state of light reflected from the surface of a sample. The measured values are expressed as psi (Ψ)and delta (Δ). These values are related to the ratio of Fresnel reflection coefficients R_p and R_s for p- and s- polarized light. Equation 3.3 shows this relationship.

$$\rho = \frac{R_p}{R_s} = \tan(\Psi)e^{i\Delta} \qquad 3.3$$

Ellipsometry can determine thin film thickness and optical constants of the same sample. One important factor is that the light beam must penetrate to the film or interface that is being studied and also have the ability to propagate back out of the sample after reflection from the interface that is, the absorption must be sufficiently low and the reflections from the interface must be sufficiently high. If this is not possible then using reflection ellipsometry for measurements is impossible.

3.4.3 Relating Mass Uptake to Refractive Index Change

Once the mass uptake of the analyte is known, the resulting change in the index of refraction of the sensor coating can be estimated. This knowledge of the refractive index change in the sensor coating permits the construction model of how the waveguide should respond to the sorption of the same analyte, and this modeling can be used to calibrate and interpret the experimental data from the waveguide sensors. The relationship between the mass uptake and the refractive index can be approximated by a dielectric mixing rule.

There are several approaches to calculate the effective refractive index of internally mixed particles using the refractive indices of the individual species. Three approaches are shown below.

a) Simple Weighted mixing: volume or mass Average

$$m_e = \sum_j m_j f_j \qquad 3.4$$

where:
m_j is the refractive index of species j
f_j is either its volume or mass fraction
m_e is the effective refractive index

b) Bruggeman approximation: used for two randomly mixed species

$$f_1 \frac{\varepsilon_1 - \varepsilon_e}{\varepsilon_1 + 2\varepsilon_e} + f_2 \frac{\varepsilon_2 - \varepsilon_e}{\varepsilon_2 + 2\varepsilon_e} = 0 \qquad 3.5$$

where:
ε_i are the dielectric constants of the two materials,
f_i are the volume fractions of the materials
ε_e is the effective dielectric constant
Note that the refractive index is the square root of the dielectric constant.

c) Maxwell-Garnett approximation: used when one species is a host material matrix with the dielectric constant and the other is an inclusion species with dielectric constant, ε_1

$$f_1 \frac{\varepsilon_1 - \varepsilon_2}{\varepsilon_1 + 2\varepsilon_2} = \frac{\varepsilon_e - \varepsilon_2}{\varepsilon_e + 2\varepsilon_2}$$
$$f_2 \frac{\varepsilon_2 - \varepsilon_1}{\varepsilon_2 + 2\varepsilon_1} = \frac{\varepsilon_e - \varepsilon_1}{\varepsilon_e + 2\varepsilon_1} \qquad 3.6$$

where:
ε_2 is the dielectric constant of the host material
ε_1 is the dielectric constant of the included species
f_i are the volume fractions of the materials
ε_e is the effective dielectric constant

The Maxwell-Garnett works well as a dielectric mixing model since the polymeric sensing material acts like a "host material" and the analyte as a relatively low concentration inclusion species. With the ability to use the spectroscopic ellipsometry method for calibrating the index change due to the introduction of the analyte to the polymeric sensing layers; this will allow experimental verification of the resulting index changes in the polymeric layers as a result of analyte absorption.

CHAPTER 4

Experimental Design and Setup for Testing

4.1 Experimental Setup

A gas delivery system has been constructed for precise control of the concentrations and flow rates of volatile analyte chemicals such that well known gas mixtures can be delivered to one of the two experimental apparatus: a waveguide test chamber and an associated quartz crystal microbalance test chamber (QCM), or an ellipsometric chamber and an associated quartz crystal microbalance test chamber. This delivery system is shown in Figure 4.1 The QCM is a highly sensitive mass monitor that can be used to collect data on the mass uptake of analytes into polymeric films, and the mass uptake data can be used to calibrate and validate the data obtained from the optical waveguide sensors, or from the polymers under ellipsometric test.

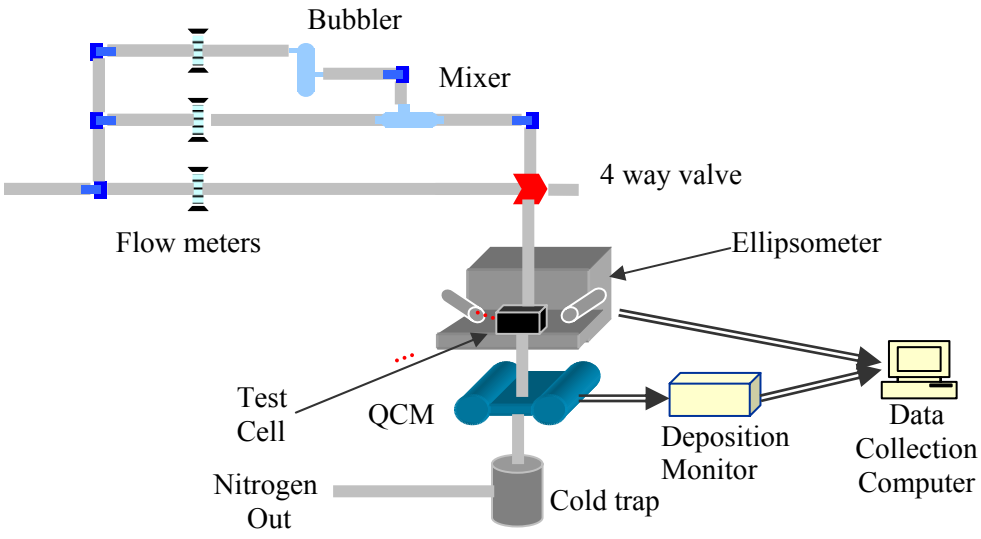

Figure 4.1: Schematic of Gas Delivery System

The delivery system is designed to use a nitrogen gas carrier stream that flows through a bubbler equipped with a sparger containing the desired chemical of interest (e.g. isopropanol, benzene, etc.). The flow of gas through the bubbler creates a saturated vapor stream of the analyte. The mass flow controllers measure the flow rate using the properties of laminar flow with a range of 0-1.2 standard cubic centimeters per minute(*sccm*) and a flow delivery accuracy of ± 0.01*sccm*. When the saturated analyte vapor stream exits the bubbler, it enters a mixing chamber where a second carrier/dilution stream of nitrogen is introduced to permit dilution and exact control of analyte concentrations in the gas stream delivered to the waveguide and QCM test chambers and high-speed, spectroscopic ellipsometer. The nitrogen is controlled by a 0-2500 *sccm* which creates a wide range of chemical vapor concentration. The chemical delivery system is able to deliver flows of methanol and similar gases between approximately 1 and 7.1 x 10^4 *ppmv*. Gas exiting the QCM/Ellipsometer was passed to a cold trap where the chemical was removed from the nitrogen stream. The cleaned nitrogen stream is then vented into the building exhaust.

Figure 4.2: Gas Delivery System

4.2 QCM Sorption Measurement

As an example of the data that can be obtained from the QCM system and used for calibration of the waveguide sensor response, a QCM sorption measurement using a polymer sensing layer and water as the analyte is presented here.

For the QCM experiments, all analyte sorption measurements are conducted using a Maxtek quartz crystal microbalance (PLO-10 Phase Lock Oscillator, 5MHz gold plated quartz crystals model # SC-501-1).

In order to ensure that the polymer film is initially dry, the polymer coated QCM crystal was placed in the testing chamber, shown in Figure 2.5, and purged with dry nitrogen for approximately 8 hours or until the frequency has stabilized. This allows the chamber to stabilize at low relative humidity value (less than 5%).

After the purge cycle, QCM mass data of the dry crystal is recorded for twenty minutes to one hour under dry nitrogen flow or as long as needed to achieve equilibrium uptake. After approximately one hour of data collection, the carrier gas stream is diverted through the chemical bubbler filled with water or another analyte to produce a saturated vapor stream or known concentration of analyte going into the QCM test chamber. QCM mass uptake data is again recorded until the mass of the coated crystal stabilized and equilibration of the polymer film and the humid nitrogen stream is achieved. Finally, humid nitrogen flow is terminated and dry nitrogen purges through the QCM test chamber. Film mass data is collected during the chemical desorption period until the mass of the coated QCM crystal again stabilizes in the dry nitrogen stream. Figure 4.2 shows the raw frequency data collected from the QCM during this testing cycle. The QCM can measure frequency changes of 0.12 *Hz* which corresponds for a 1-

um-thick film of HFAPNB, to a mass per unit area resolution of 1.56 ng/cm^2. The QCM allows the mass uptake of an agent to be accurately linked to a chemical concentration.

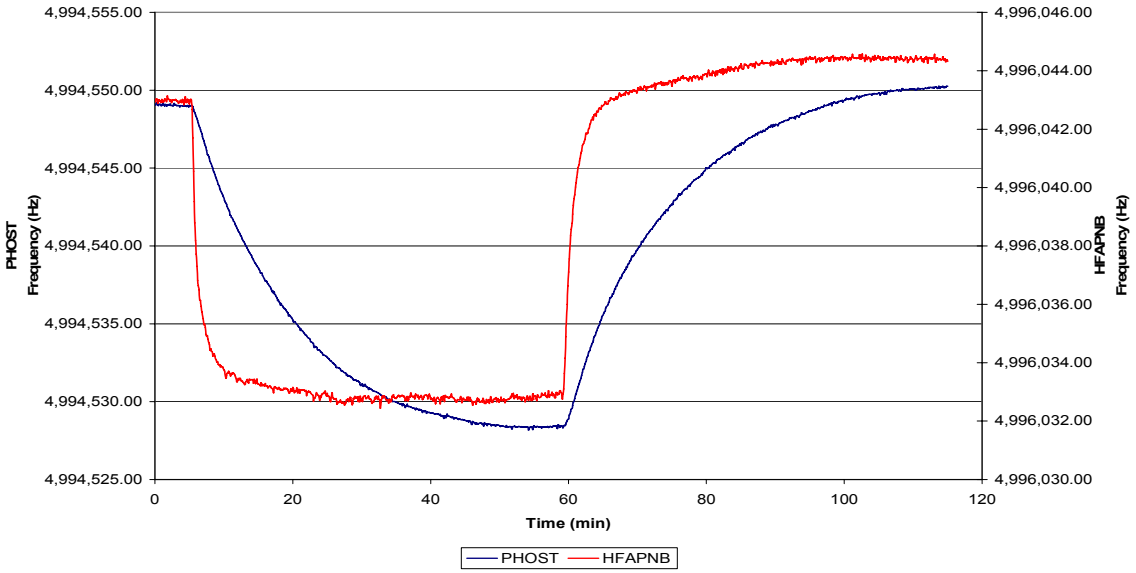

Figure 4.3: Basic frequency shift due to an uptake of a specific analyte which was introduced into the test chamber.

As shown in Figure 4.2, the polymer coated QCM crystals were initially allowed to reach equilibrium with nitrogen flowing and the relative humidity less than 5% (dry conditions) which is indicated by the initial flat line. After baselining at the dry conditions, a saturated water or alcohol vapor stream is delivered into the QCM test chamber. After reaching equilibrium in the wet conditions, pure nitrogen was again delivered to the chamber until the QCM reached equilibrium. Here, a decrease in the QCM crystal frequency represents mass uptake into the polymer film coating the crystal due to the sorption of an analyte. An increase in the frequency represents mass loss from

the polymer due to desorption. The raw frequency data is now analyzed using the Sauerbrey equation to find to the total weight % uptake and diffusion coefficients.

4.3 Film Thickness Measurements

A variable angle spectroscopic ellipsometer (M2000 V-Vase from J.A. Woollam Inc.) was used to measure the thickness of the different polymer films used in these experiments. For these measurements, the materials of interest were cast onto plain silicon wafers (Nova Electronics Materials) or onto the gold plated QCM crystals. The ellipsometry parameters ψ and Δ were collected over the wavelength range from 500 nm to 1000 nm at an angle of 65°. The ψ and Δ were analyzed using the WVASE-32 analysis software (J.A. Woollam Inc.) by fitting the ellipsometry data to a film stack model composed of a Cauchy layer model for the polymer film on top of a 15 angstrom thick SiO_2 layer, all on a semi-infinite layer of silicon. For the QCM crystal film thickness, a Cauchy layer model was used on top of a semi-infinite layer of gold. To insure that the polymer film was dry a test chamber for the ellipsometer shown in Figure 4.4 was also custom designed to allow the polymer coated silicon wafer to be introduced to a saturated vapor stream coming from the delivery system.

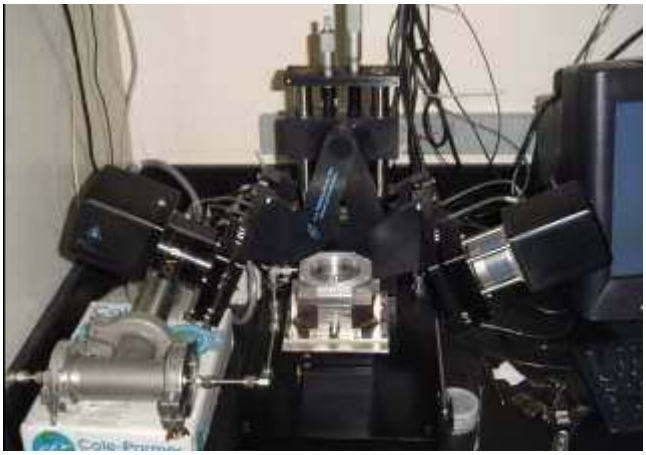

Figure 4.4: Ellipsometer and QCM test chamber. The chamber containing the QCM is to the left of the ellipsometer

Figure 4.5 below shows a typical response of the ellipsometer for the change of refractive index and polymer thickness due to an introduction of a chemical, in this case, methanol. Again the same conditions are applied as stated above for the introduction of an analyte into the test chamber of the ellipsometer. The test chamber is flooded with pure nitrogen to insure a dry condition for initial testing, then the 4-way valve is switched to introduce the saturated vapor stream into the test chamber which holds the polymer coated silicon wafer. After the system is introduced with a new analyte, it is allowed to equilibrate. These testing procedures where repeated for each experiment. Both the mass uptake and ellipsometric data are collected simultaneously to ensure identical conditions.

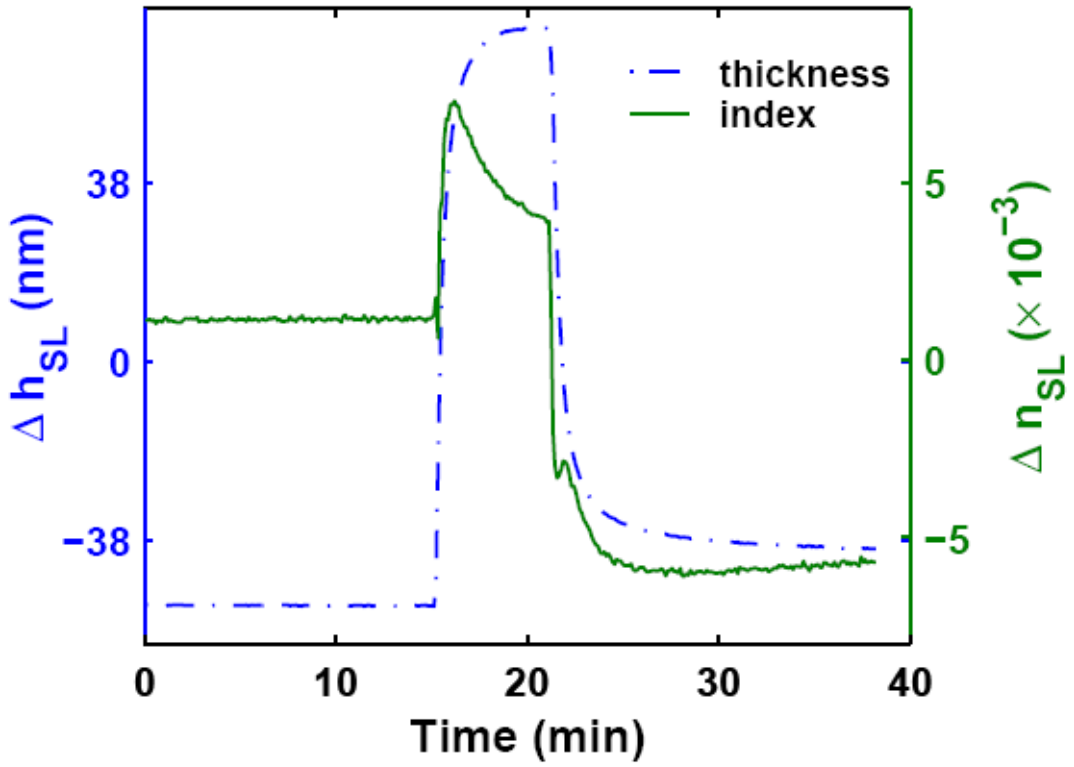

Figure 4.5: Change of refractive index and thickness of HFAPNB polymer in response to saturated methanol stream

As the methanol is absorbed into the polymer and displaces air there is a sharp peak followed by a gradual fall. This initial increase then fall suggests that initial displacement of air is occurring. The lower-index methanol stretches the polymer, decreasing the relative amount of polymer to methanol and therefore the index. This deformation ultimately affects sensor response.

CHAPTER 5

Results

5.1 Data Collection

Using the apparatus described earlier, the response of HFAPNB and PHOST to different concentrations of analytes has been characterized. These analytes consisted of methanol, isopropanol, benzene and water. For each analyte the two polymers of interest where characterized by finding the refractive index shift, the mass uptake and the thickness increase as they changed over time for different concentrations of the analytes. It is proposed that by configuring an array of different polymers it is possible to detect the amount of an unknown analyte and its concentration. This will be demonstrated below through a series of different experiments and a simple mathematical model to determine the concentration of two analytes in solution.

5.1.1 Dry Film Mass Estimation

A quartz crystal microbalance (QCM) was used to measure the mass of analyte added to polymer films when exposed to environments of differing analytes. A QCM utilizes oscillating quartz crystals as a means for mass measurement. By monitoring the changes in the oscillation frequency of the polymer coated quartz crystal, it is possible to monitor the absorption and desorption of water or any other analyte from the film.

The first experiments conducted were to determine the calculated “dry” mass which will be used to estimate the overall mass gain due to water sorption rather than actual water content of the film. This was completed by measuring the frequency shift of

the polymer coated QCM crystals to varying relative humidity environments. This data was used to correlate the relationship between the water partial pressure in the environment and the QCM frequency. Figure 5.1 shows the linear fit of the HFAPNB date with an R^2 value of 1.00. The y-intercept should be in theory the frequency of the polymer coated crystal in a completely dry environment. This value can be used later to calculate the dry mass of the polymer thin film. In theory there will most likely be small quantities of water tightly bound to the polymer matrices that would skew this calculated dry mass. For the purpose of this paper, the calculated value for the estimated dry mass of polymer will be sufficient for any calculations. This same experiment was conducted on PHOST and similar results were obtained and can be found in the appendix.

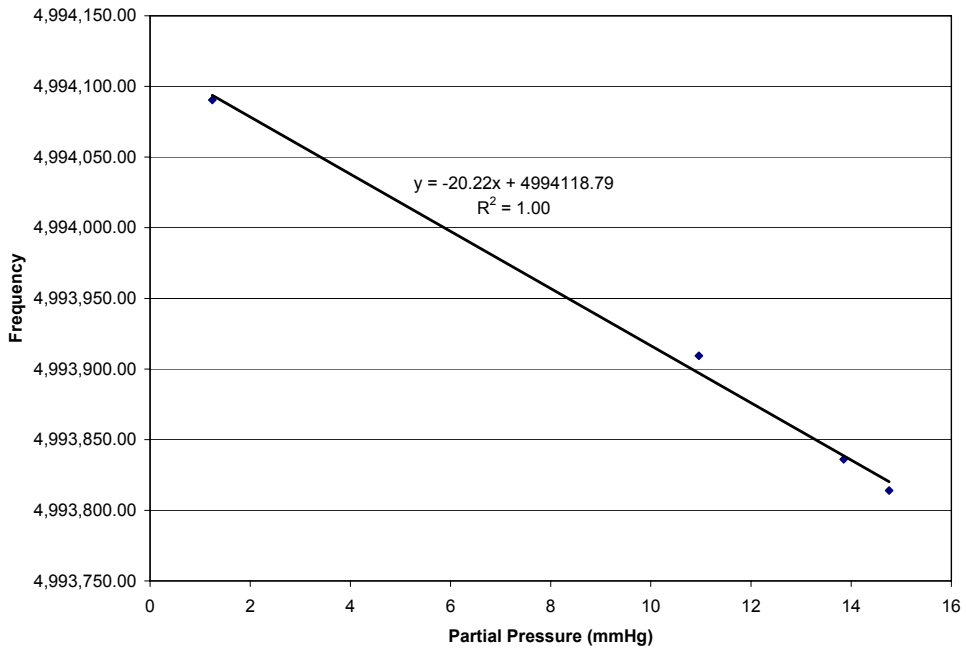

Figure 5.1: Linear relationship between QCM crystal frequency for HFAPNB and water partial pressure.

The natural frequency of the QCM crystal used in each experiment was measured prior to being coated with the polymer film. The mass of material on the crystal can then be calculated from the various QCM frequency values by using equation 5.1, which is a variation of the Sauerbrey equation.

$$m_{added} = \frac{(f_{uncoated} - f_{measured})}{C_f} \qquad 5.1$$

In this equation, m_{added} is the mass added to the crystal per unit area, $f_{uncoated}$ is the natural frequency of the clean crystal, $f_{measured}$ is the frequency of the crystal after some mass is added to the crystal's surface, and C_f is a constant. The C_f is defined as the mass sensitivity or calibration constant of the QCM and is independent of the physical properties of the deposited material. This constant was discussed in Chapter 3. It is important to understand that the Sauerbrey equation above has limitations. It is only valid for thin films that can be considered rigid masses. This is because the small amounts of mass added to the quartz crystal can be treated as equivalent thicknesses of quartz. If the film is not a rigid mass, the shear wave in the QCM crystal will lose significant amount of energy through visco-elastic losses in the non-rigid mass. This energy loss effects the frequency measurement and the crystal behavior can deviate strongly from the Sauerbrey relationship. The absolute accuracy of the QCM is predicated by the accuracy of the formula used to convert the frequency measurements to mass change.

5.1.2 Equilibrium uptake for Methanol, IPA, Benzene and Water at different concentrations

Again, the precision gas-mixing system, which produced a precise concentration of an analyte, was used to determine the mass percent uptake in both HFAPNB and PHOST. Experiments were conducted with different concentrations of methanol, ispropanol, benzene and water ranging from 0 and 7.1 x 10^4 *ppm*. Figure 5.4 shows a representation of the change in frequency for both PHOST and HFAPNB due to different concentrations of water. This was a continuous experiment where the QCM chamber was supplied with water at 44, 88, and 177ppm. After each concentration there was a continuous stream of nitrogen to purge the system of any water. As the frequency decreases, this is a representation of the analyte being absorbed into the polymer or a mass uptake of analyte. As the frequency increases, a valve in the gas delivery system was switched to where pure nitrogen was introduced into the QCM chamber.

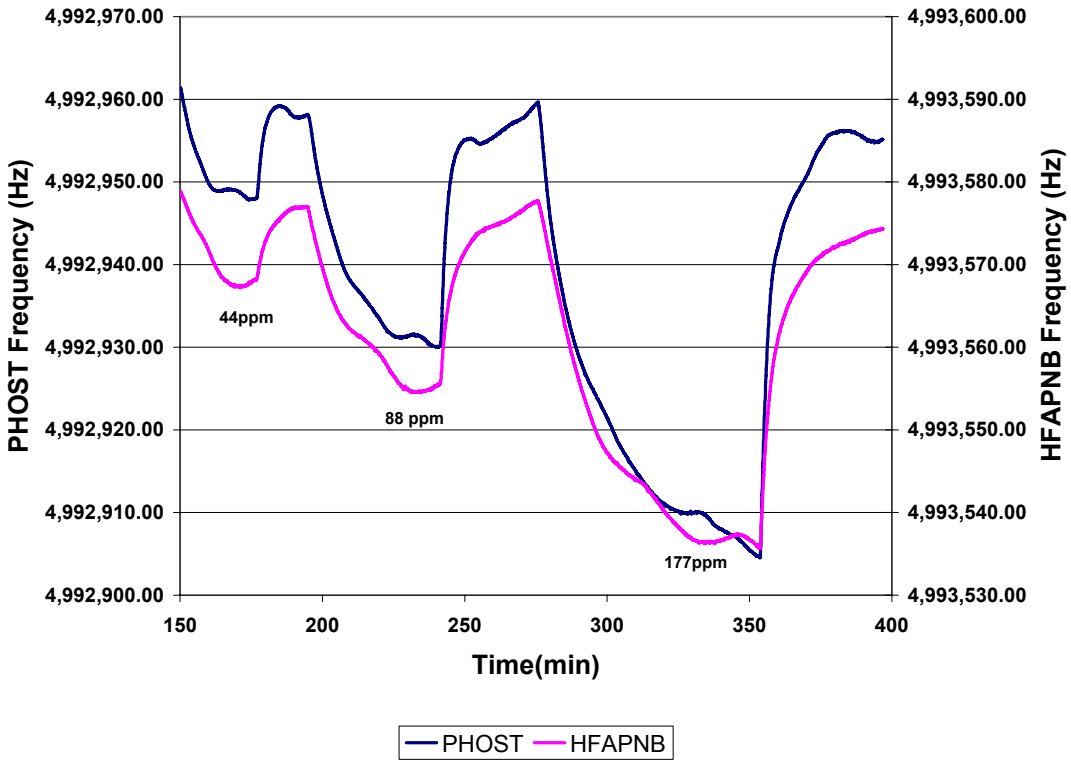

Figure 5.2: Frequency shifts of PHOST and HFAPNB due to different concentrations of water.

This same experiment was conducted on both polymers with other analytes such as methanol, isopropanol and benzene. The raw data for each analyte is shown in Appendix A. Table 5.1 shows the mass percent uptake at different concentrations for these analytes. Dashes in the table represent that there was no sensitivity of the polymer to the analyte that was introduced in the chamber, or that there was a negative effect. For example, the frequency increases suggesting that mass is lost while the chosen analyte is flowing through the system. This mass is not quantifiable to an amount of analyte absorbed by the polymer.

Table 5.1: Comparison of different mass percent uptake with water, methanol, isopropyl alcohol, and benzene at different concentrations

Concentration(ppm)	Mass % uptake PHOST	Mass % uptake HFAPNB
Water		
44	0.14	0.11
88	0.31	0.22
177	0.6	0.44
144,000	6.56	6.13
Methanol		
3	------	0.019
10	------	0.032
56	------	0.056
112	0.04	0.1
224	0.22	0.27
150,000	41	32
Isopropyl Alcohol		
0.98	------	0.014
3.5	------	0.029
20	0.027	0.168
39	0.147	0.44
78	0.24	1.18
49,000	43.37	43.93
Benzene		
8	-------	0.07
45	-------	0.27
91	0.06	0.47
68,000	4.76	22.18

By utilizing the data in Table 5.1 we are able to understand if the equilibrium uptake for each polymer film and analyte combination has a characteristice linear or non-linear uptake. Figure 5.3 below shows the linear uptake for water while Figure 5.4 shows the non-linear uptake for methanol.

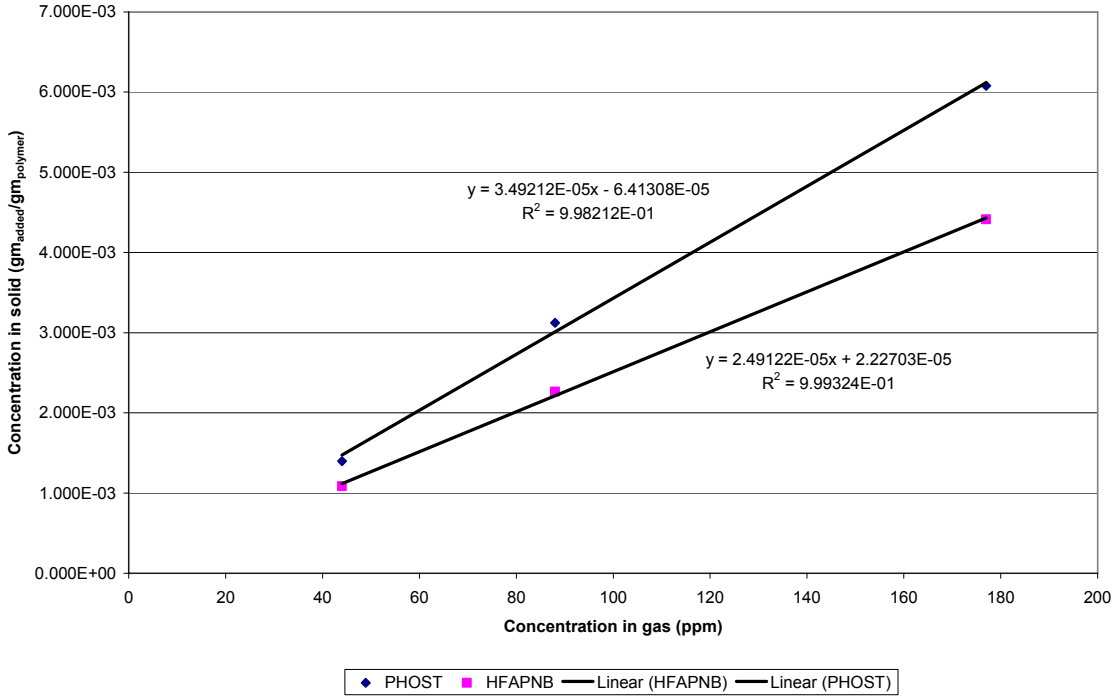

Figure 5.3: Interaction Model for PHOST and HFAPNB of Water

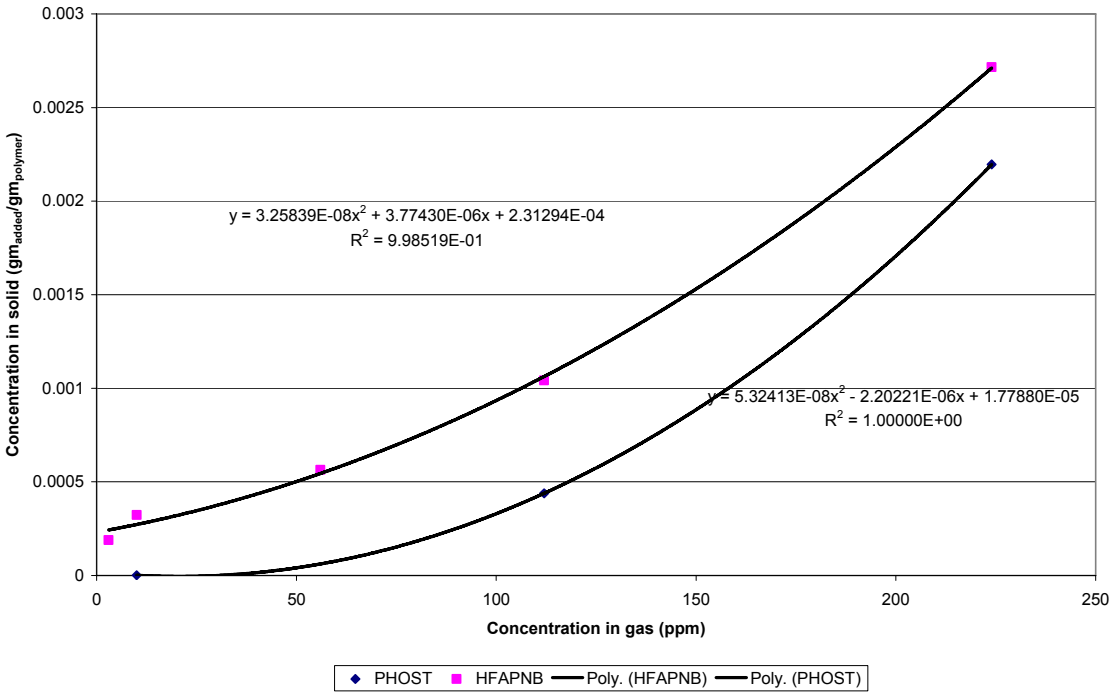

Figure 5.4: Interaction Model for PHOST and HFAPNB of Methanol

Table 5.2 shows the relationship for each combination of film and analyte. Note that equilibrium uptake for water is linear in both HFAPNB and PHOST and non-linear for methanol uptake.

Table 5.2 Comparison of interaction models for PHOST and HFAPNB with water, methanol, isopropyl alcohol and benzene

Interaction Model $y = ax^2 + bx + c$ or $y = mx + c$	**PHOST**	**HFAPNB**
Methanol	$a = 5.324 \times 10^{-08}$ $b = 2.202 \times 10^{-06}$ $c = 1.778 \times 10^{-05}$	$a = 3.258 \times 10^{-08}$ $b = 3.774 \times 10^{-06}$ $c = 2.313 \times 10^{-04}$
Isopropanol	$a = 1.00 \times 10^{-08}$ $b = 3.14 \times 10^{-05}$ $c = -4.21 \times 10^{-05}$	$a = 1.32 \times 10^{-06}$ $b = 7.43 \times 10^{-05}$ $c = 4.57 \times 10^{-05}$
Benzene	$a = 1.34 \times 10^{-11}$ $b = 8.15 \times 10^{-08}$ $c = 6.31 \times 10^{-04}$	$m = 4.65 \times 10^{-06}$ $c = 2.51 \times 10^{-03}$
Water	$m = 3.49 \times 10^{-05}$ $c = -6.41 \times 10^{-05}$	$m = 2.49 \times 10^{-05}$ $c = 2.23 \times 10^{-05}$

In Table 5.2 the y-variable correlates to the mass added in the polymer film while the x-variable denotes the concentration of the analyte.

Both PHOST and HFAPNB used in this study contain hydroxyl functional groups that are hydrophilic and capable of hydrogen bonding to some degree. Because of this similarity in hydrogen bonding sites, it is thought that the polymers studied are capable of absorbing significant quantities of analytes. However, there are some differences in the amount of analyte sorbed at saturation for each polymer. This difference in the amount of sorbed material can be a result of various factors including the free volume differences between materials and differences in the affinity or solubility of analytes in the polymers. By not assuming that our polymers are rigid masses, and instead a viscoelastic material, when a stress is applied, parts of the long polymer chain can change position. This movement or rearrangement is called creep. Polymers remain a solid material even when parts of their chains are rearranging in order to accompany the stress, and as this occurs, it creates a back stress in the material. When the back stress is the same magnitude as the

applied stress, the material no longer creeps. When the original stress is taken away, the accumulated back stresses will cause the polymer to return to its original form. The introduction of these stresses coupled with the solubility of analytes in the polymer could explain the differences in the wt% uptake of methanol, isopropanol and benzene as compared to water.

5.1.3 Estimation of Analyte Diffusion Coefficients in HFAPNB and PHOST

To estimate the diffusion coefficients for the different analytes in the two polymers of interest, the raw QCM frequency data is converted to mass uptake. With mass uptake data, relative mass uptake versus the square root of time is plotted. The initial linear region for relative mass uptakes less than 0.6 indicates Fickian diffusion behavior. If purely Fickian diffusion is occurring during these processes, the diffusion behavior and water uptake can be modeled using the following equation,

$$\frac{M_t}{M_\infty} = 1 - \frac{8}{\pi^2}\sum_{n=0}^{\infty}\frac{1}{(2n+1)^2}\exp\left[-\frac{(2n+1)^2\pi^2 Dt}{4L^2}\right] \qquad 5.2$$

where M_t is the mass uptake at time t, M_∞ is the ultimate mass uptake at time $t = \infty$, D is the diffusion coefficient (cm^2/s), and L is the film thickness. For the initial linear phases of the sorption process ($M_t/M_\infty < 0.6$), a simplified version of equation 5.2 can be used that describes mass uptake into a thin, semi-infinite slab from one face. This shows that the uptake for polymers is observed to follow a linear relationship versus the square root

of time. This can only be used during the initial uptake times and is related to M_t/M_∞ <0.6.

$$\frac{M_t}{M_\infty} = \frac{2}{L}\left(\frac{Dt}{\pi}\right)^{\frac{1}{2}} \qquad 5.3$$

This equation is often referred to as the "short time" equation and was used to estimate a Fickian diffusion coefficient of the various polymers studied. Fractional mass uptake (M_t/M_∞) was plotted against $t^{1/2}$ and the slope of the resulting plot was used to evaluate D. After calculating the fractional mass uptake (M_t/M_∞) from the QCM frequency data and plotting against $t^{1/2}$, the resulting slope from $M_t/M_\infty = 0$ to $M_t/M_\infty = 0.6$ was found to calculate the Diffusion coefficient, D. In conjunction with estimating the diffusion coefficients for the short time approximation, a least squares fit analysis was also completed on the data by utilizing equation 5.2 and optimizing on the diffusion coefficient and time lag of the experiment. The diffusion coeffienct attained with this analysis is a reflection for the complete sorption of analyte and not an approximation from $M_t/M_\infty <= 0.6$. Figures 5.5-5.7 illustrates the fractional mass uptake versus the square root of time for both PHOST and HFAPNB for analytes methanol, IPA and benzene and compare data to a theoretical Fickian mass uptake model. The correlating diffusion coefficient and mass % uptake at saturation is also shown. The design of the gas delivery system introduced a time lag within the experiment. Again by using the

least squares fit tool, the theoretical time lag has been estimated for each polymer/analyte combination.

As briefly discussed before and as can be seen from Figures 5.5-5.7, there is a time lag difference from the theoretical model compared to the experimental data. This time lag is caused by the design setup of the experiment. Table 5.3 below shows the calculated value of each analytes time lag. By comparing the diffusion coefficients for the theoretical model and the short time approximation, all are close to the short time approximation number. The slight differences could be associated to the time lag and observances were that the full time approximation was usually slightly lower than the short time approximation, or a mass transfer resistance at the interface.

Table 5.3: Time lag values for Methanol, IPA and Benzene at saturation values.

Time Lag (sec)	PHOST	HFAPNB
Methanol	147	16
Isopropanol	58	99
Benzene	32	22
Water	16	5

As shown in Figure 5.5 there is a slight difference in rate of uptake between the two polymers of choice, PHOST and HFAPNB. Figure 5.5 graphically depicts the diffusion coefficient differences between the two polymers. By understanding the difference in diffusion properties of the two polymers, it is proposed that the concentration of a mixture of two analytes can be determined. This will be discussed later.

Table 5.4: Diffusion Coefficients and Mass % Uptake for methanol in PHOST and HFAPNB at Saturation (150,000ppm)

	Diffusion Coefficient (Full Model) cm^2/sec	Diffusion Coefficient (Short Time Approximation) cm^2/sec	Mass % Uptake
PHOST	8.13×10^{-10}	2.192×10^{-9}	41
HFAPNB	5.69×10^{-9}	4.523×10^{-9}	32

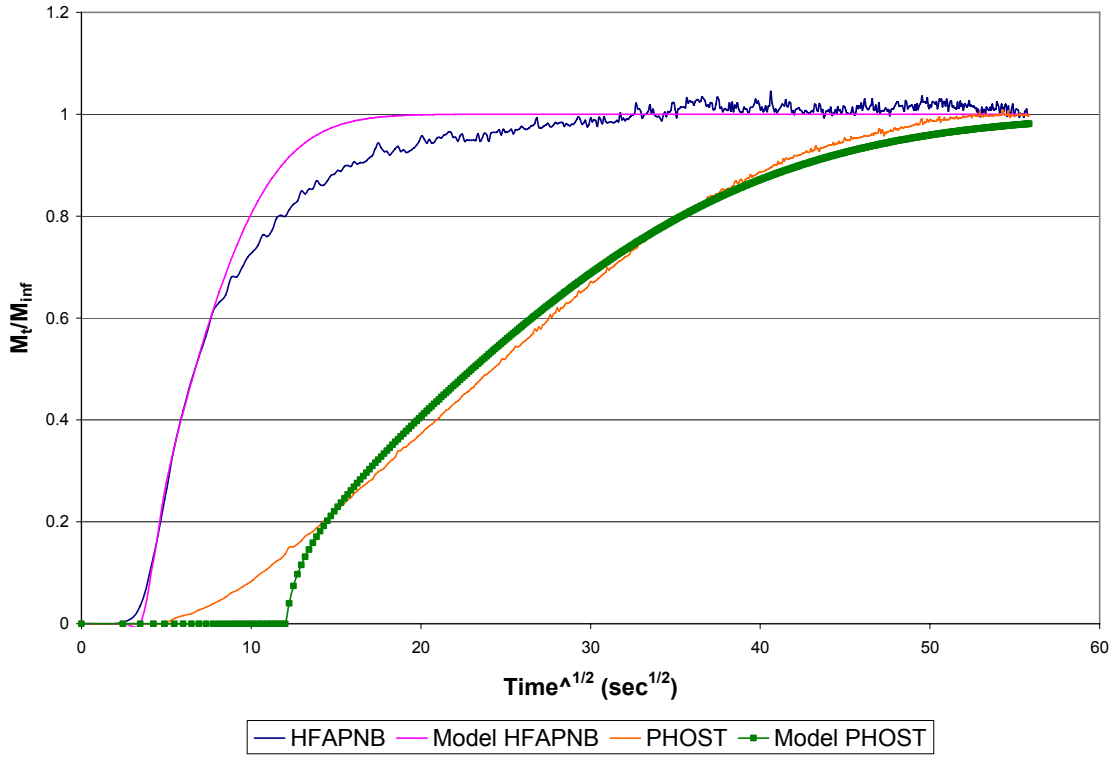

Figure 5.5: Comparison of rate of uptake between HFAPNB and Phost in methanol

Table 5.5: Diffusion Coefficients and Mass % uptake for Isopropyl Alcohol in PHOST and HFAPNB at Saturation (49,000ppm)

	Diffusion Coefficient (Full Model) cm^2/sec	Diffusion Coefficient (Short Time Approximation) cm^2/sec	Mass % Uptake
PHOST	1.039×10^{-9}	1.613×10^{-9}	43.37
HFAPNB	1.721×10^{-9}	1.926×10^{-9}	43.93

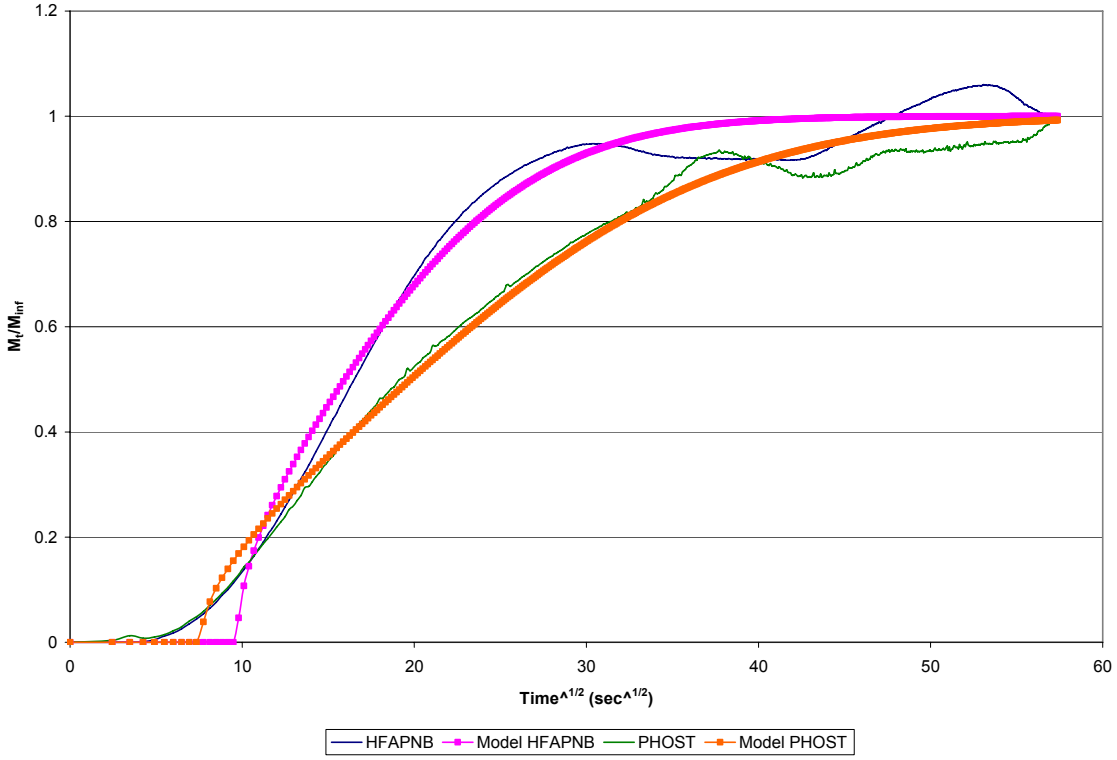

Figure 5.6: Comparison of rate of uptake and % mass uptake for Isopropyl Alcohol in PHOST and HFAPNB

By examining the diffusion coefficients of the IPA to methanol to benzene there does not seem to be that significant of a difference(all are relatively on the same order of magnitude), but the difference comes in at the amount of mass uptake. With IPA there is a little more than 40% increase in mass uptake, while methanol has a range from 32-41% mass uptake. This seams fairly congruent since both analytes in question are small molecules. As the analyte changes to benzene however, the mass % uptake changes dramatically. It appears that the HFAPNB and PHOST have similar sensitivity to IPA and methanol, however, when observing benzene this is not the case. The diffusion coefficient are on the same magnitude, however the mass percent uptake is 4.65 times

larger for the HFAPNB polymer compared to the PHOST polymer. Both polymers have a relatively polar matrix that has an affinity for polar compounds.

Table 5.6: Diffusion Coefficients and Mass % uptake for Benzene in PHOST and HFAPNB at Saturation (114,000ppm)

	Diffusion Coefficient (Full Model) cm^2/sec	Diffusion Coefficient (Short Time Approximation) cm^2/sec	Mass % Uptake
PHOST	2.267×10^{-9}	4.12×10^{-9}	4.76
HFAPNB	5.397×10^{-9}	7.317×10^{-9}	22.18

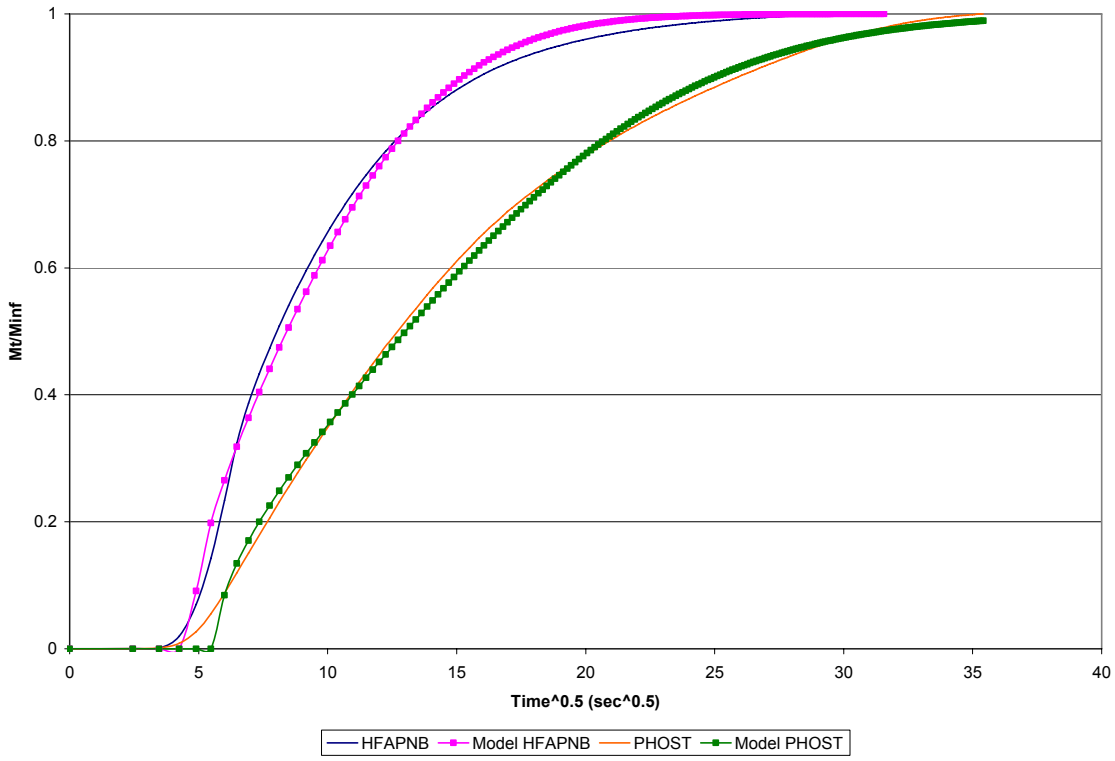

Figure 5.7: Comparison of rate of uptake and % mass uptake for Benzene in PHOST and HFAPNB

It could be concluded that the uptake of benzene in the PHOST polymer was minimized because of two benzene rings being in close proximity of each other resulting in available bonding sites being masked. In HFAPNB the bis-trifluoromethyl carbinol group, which provides a strong hydrogen bonding to polar compounds, is attached to the bridged cyclic hydrocarbon, but because of the size of the functional group it has the ability to have more bonding sites available. This is shown in Table 5.6 by the difference in mass uptake between the PHOST polymer and HFAPNB when benzene is the analyte of choice.

The differences from the theoretical model to the experimental model could be attributed to the assumptions around the Sauerbrey equation. As discussed earlier, the assumption was made that our polymer thin film was considered a rigid mass. However, as the analytes are absorbed into the polymer films, plasticizing them, this could change their elastic behavior. This change in elastic behavior of the polymer film can have significant deviation from the Sauerbrey equation. The existence of tensile stress in the film can cause the resonant frequency of the quartz crystal to change from that in a stress free state. The experimental data shown above thus demonstrates that for the precise determination of mass with a QCM, the elastic properties of the deposited material more than likely should be taken into consideration. The greater accuracy of mass loading can be achieved by incorporating the acoustic impedance of the material. A good indicator of the elastic behavior of the quartz crystal/polymer film system is the ratio of the acoustic impedance (Z) of the respective materials. As the elastic behavior of the polymer film changes, the value of Z will change as well. For high mass loadings on a QCM significant deviations from the Sauerbrey equation can occur for small changes in Z.

It was also assumed that the diffusion of the penetrants through the polymers followed the standard Fickian model which might not be the case. Deviations of Fickian behavior are considered to be associated with the finite rates at which the polymer structure may change in response to the sorption or desorption of penetrant molecules. These non-Fickian effects may be related to the influence of the changing polymer structure on solubility and diffusional mobility, or result from the internal stresses exerted by one part of the polymer film on another as diffusion proceeds. Another assumption was that the diffusion coefficients where constant when in fact they could be concentration dependent diffusion coefficients.

5.1.4 Gas Phase Mixing Model for Estimating Diffusion Coefficients

The previous paragraphs have discussed the different diffusion coefficients for water, methanol, isopropanol and benzene. It has also been shown the different mass % uptakes relative to a certain analyte concentration delivered by the gas delivery system. We have previously analyzed our experimental data and evaluated it against the purley Fickean diffusion uptake equation 5.2. This section will now treat the gas space above the QCM crystal as a continuous stirred tank reactor(CSTR) and evaluate the model against our experimental data. Concentration of the gas at any time (t) can be computed by equation 5.4.

$$C_{gas}(t) = (1 - e^{t/\tau})C_{nominal} \qquad 5.4$$

The mass balance of our system yields

$$D\frac{\partial^2 C}{\partial x^2} - \frac{\partial C}{\partial t} = 0 \qquad 5.5$$

The boundary conditions for this equation are as follows

- Initial Boundary Condition: C(x) = 0 everywhere for t=0
- Boundary Condition (1): dC/dx (x=0) =0 for all t
- Boundary Condition (2): C(x=L)= H(Cgas(t))

The assumptions associated with the design model are that

1) The surface concentration of film equilibrates with the gas phase instantly(ie. no mass transfer resistance at the interface)
2) Impermeable bottom boundry—BC1
3) The Diffusion coefficient is constant over the time of the absorption
4) The gas space above the QCM crystal can be treated like a CSTR

Equation 5.5 was solved by using the finite difference methods for parabolic equations by using MatLab. The MatLab code can be found in the Appendix. The H*C variable in BC2 is simply the interaction models found from the $M_t/M(polymer_{analyte})$ vs $C_{analyte}$ curve and recorded in Table 5.2. This is very similar to the Henry constants that are found in vapor liquid equilibrium. If you assume that the vapor and liquid are in equilibrium it is possible to find the concentrations in each phase through this constant. For example, Henry's law constant can expressed as the dimensionless ratio between the aqueous-phase concentration c_a of a species and its gas-phase concentration c_g as shown in Equation 5.6

$$K_h^{cc} = c_a / c_g = k_H \times RT \qquad 5.6$$

where: R = gas constant
T = temperature.

Similar to this, the models established for this experiment were correlated to the slope of the mass uptake at time t, (M_t) to the ultimate mass uptake at time $t = \infty$ (M_∞) versus the concentration of the analyte, which is shown below in Equation 5.7. This H variable is characteristic of the specific interaction between a particular absorbent and a particular adsorbate.

$$H_{Polymer_{analyte}} = \frac{(M_t / M_{Polymer_{analyte}})}{C_{analyte}} \qquad 5.7$$

Since the H constants are specific to the type of polymer used and the analyte that is being detected, these values were determined experimentally and discussed earlier in section 5.1.2. Figure 5.8 below shows the results of experimental data for methanol compared to the gas phase mixing model discussed above.

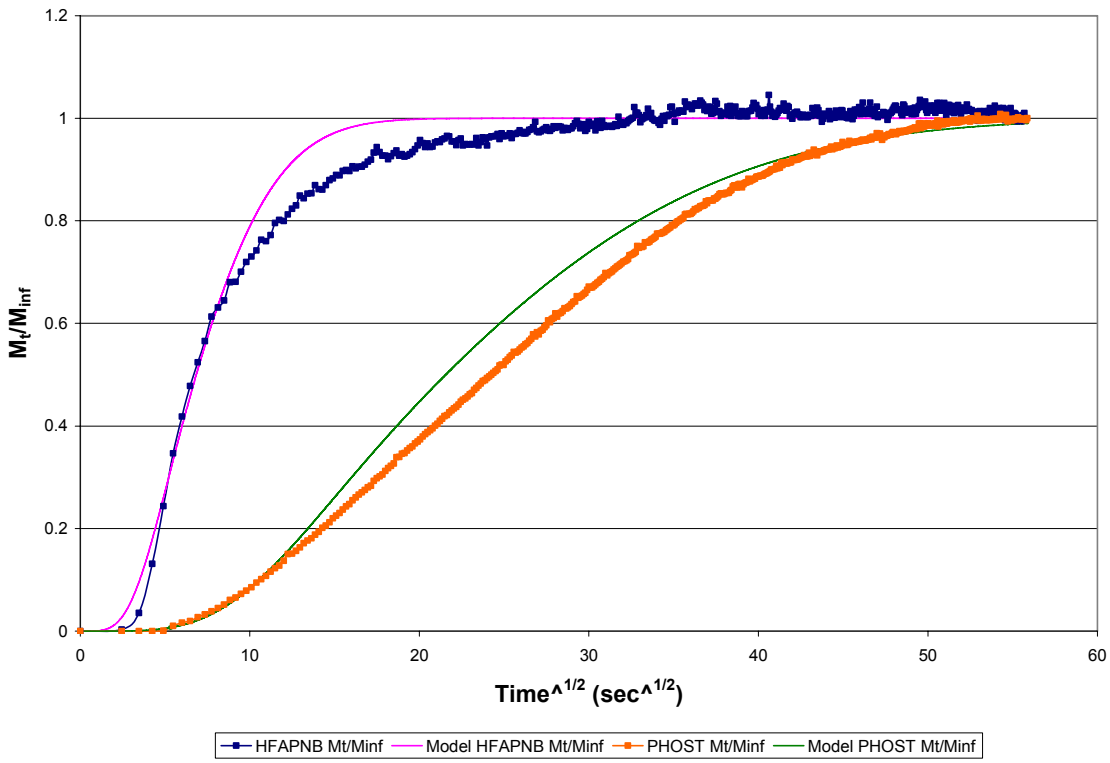

Figure 5.8: Comparison of experimental data and CSTR model for Methanol in both PHOST and HFAPNB

As seen above in Figure 5.8, the HFAPNB polymer gives a similar uptake during the linear portion of the mass uptake curve and then has a positive deviation from the experimental data. This could suggest that the diffusion coefficients are concentration dependent. This type of deviation was observed to varying degrees for all the polymers used in this work. At the beginning of the experiment where M_t/M_∞ is less than 0.2 there is also a deviation from the experimental data which might suggest that as the analyte was introduced into the system, the flow over the QCM head space had an initial boundary layer issue or that there was some mass transfer resistance at the interface. Deviations from the the PHOST polymer could also suggest concentration dependent

diffusion coefficients. Comparisons of exprimental data and CSTR model for other analytes such as IPA, Water, and Benzene are shown in the appendix.

5.1.5 Experimental Results versus Mathematical model

This section will discuss specifically if it is viable to determine the concentration of a 50/50 molar mixture of methanol and water. It is proposed that by using two sensing layers for detection, PHOST and HFAPNB, the concentration of an analyte can be determined. Graphical representation of differences in the rate of uptake between water and methanol in HFAPNB and PHOST is shown below in Figure 5.9 and Figure 5.10 respectively. This further lends support that the concentration of a mixture of analytes can be recovered.

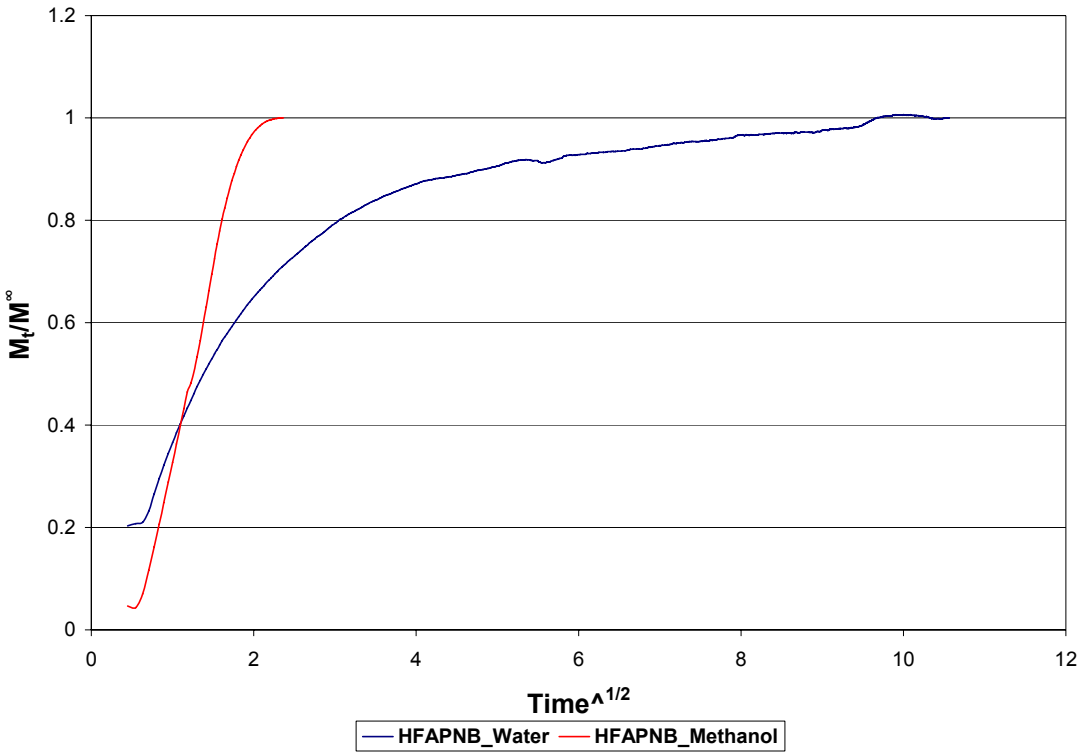

Figure 5.9: Comparison of rate of uptake between water and methanol in HFAPNB

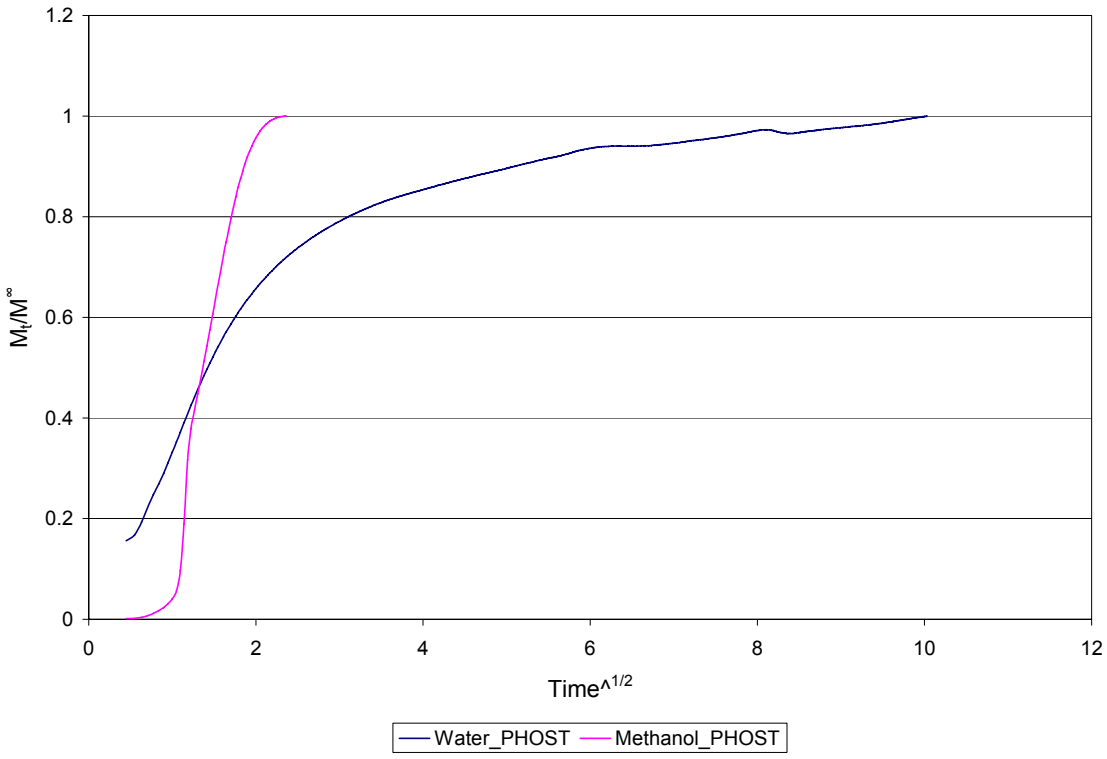

Figure 5.10: Comparison of rate uptake of methanol and water in PHOST

By utilizing the water and methanol interaction models(H*C variable) as previously described and the final mass uptake and starting film weight, it is concluded that the experimental concentration of a mixture of methanol and water as seen by the uptake in PHOST and HFAPNB can be calculated. This can be achieved by solving equations 5.8 and 5.9 simultaneously.

$$m_{PHOST} = m_{DryPHOST} + m_{DryPHOST}(H_{PHOST_{H_2O}})C_{H_2O} + m_{DryPHOST}(H_{PHOST_{MeOH}})C_{MeOH} \qquad 5.8$$

$$m_{HFAPNB} = m_{DryHFAPNB} + m_{DryHFAPNB}(H_{HPAPNB_{H_2O}})C_{H_2O} + m_{DryHFAPNB}(H_{HFAPNB_{MeOH}})C_{MeOH} \qquad 5.9$$

It was imperative to understand the concentration of the mixture of methanol and water to determine if the sensor was correctly detecting the analytes. To determine the concentration of the 50/50 molar mixture of methanol and water, the Wilson equation was utilized. For a system at equilibrium, the criterion for phase equilibrium is the equality of chemical potentials of each component in all coexisting phases. For an isothermal system this will reduce to the equality of activity coefficiens of each component in different phases. Equation 5.10 and 5.11 below represents the Wilson Equation. The Wilson equation contains just two parameters for a binary system, Λ_{12} and Λ_{21}.

$$\ln \gamma_1 = -\ln(x_1 + x_2\Lambda_{12}) + \left(\frac{\Lambda_{12}}{x_1 + x_2\Lambda_{12}} - \frac{\Lambda_{21}}{x_2 + x_1\Lambda_{21}}\right) \quad 5.10$$

$$\ln \gamma_2 = -\ln(x_2 + x_1\Lambda_{21}) + \left(\frac{\Lambda_{12}}{x_1 + x_2\Lambda_{12}} - \frac{\Lambda_{21}}{x_2 + x_1\Lambda_{21}}\right) \quad 5.11$$

Where,

$$\Lambda_{12} = \frac{v_2^L}{v_1^L}\exp\left(-\frac{\lambda_{12} - \lambda_{11}}{RT}\right) \quad 5.12$$

$$\Lambda_{21} = \frac{v_1^L}{v_2^L}\exp\left(-\frac{\lambda_{21} - \lambda_{22}}{RT}\right) \quad 5.13$$

The interaction energy between components *i* and *j*, $\lambda_{ij} = \lambda_{ji}$ was obtained from Perry's Chemical Engineering Handbook. By solving equation 5.12 and 5.13 with Wilson's Binary-Interaction Parameters, and plugging these values into equation 5.10 and 5.11, one can obtain the activity coefficients of the two analytes, methanol and water in a 50/50 molar mixture. By knowing the activity coefficients it is easy to obtain the concentration of the mixture. For this experiment, the concentration of methanol was 151ppm and the concentration of water was 37ppm.

With the concentration of the mixture known, equations 5.8and 5.9 can be solved. Instead of solving for a single real solution, it is proposed to solve over a range of methanol and water concentrations that would satisfy the equation. In doing this the sum of squares error was generated with a plot of concentration solutions that satisfies Equations 5.8 and 5.9. Figure 5.11 below gives a graphical representation of the solutions where the lowest SSE, 1.13 is at a concentration of methanol of 220ppm and water at 2ppm. The SSE at the VLE concentration of the gas, as calculated by the Wilson Equation above, is 18.1.

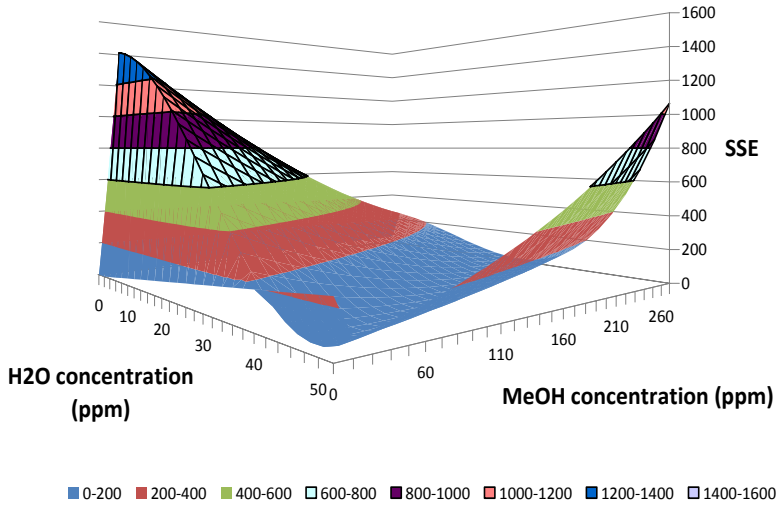

Figure 5.11: SSE plot for solutions that satisfy Equation 5.8 and 5.9 for 50/50 molar mixture of methanol and water.

Figure 5.12 shows a box plot of the difference between the experimental data and the model concentration. There is a drastic difference in the model data versus the experimental data. This difference could be contributed to a few things such as, temperature dependence of the polymer, and a small sample size to determine the H models, but more importantly the interaction of the MeOH and water within the solution and the limited number of bonding sites within the polymer. As MeOH and water compete for the bonding sites, it could be concluded that methanol is more electronegative and could mask any water uptake. Another assumption that was made was that the uptake of water and methanol were independent of each other and did not

have any interaction. By assuming this, equations 5.8 and 5.9 above were created. And results of this linear super position of the sorption equations are shown in Figure 5.11. As shown by the difference from experimental to model, the assumption that the uptake of methanol and water do not have any interaction might not be correct. In reality there is some interaction and equation 5.8 and 5.9 would need to reflect this by incorporating an interaction term for methanol and water.

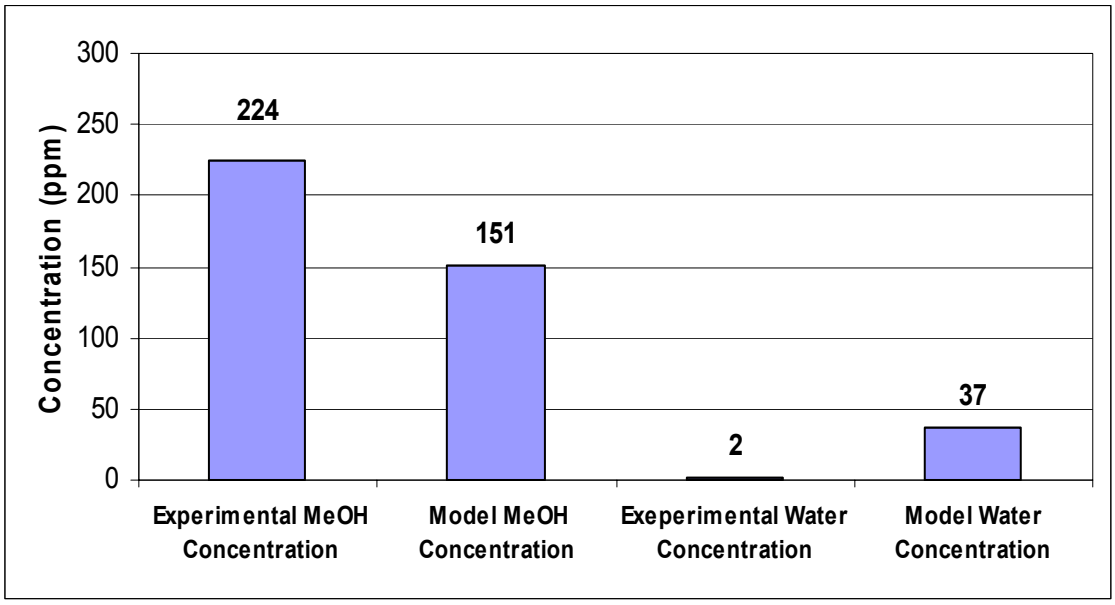

Figure 5.12: Comparison of Experimental and Model Concentration of Water and Methanol Sorption in HFAPNB and PHOST

Figure 5.13 below shows the overall mass uptake vs square root of time. By again utilizing the short time approximation and finding the diffusion coefficient for the mixture of methanol and water, a theoretical model was calculated.

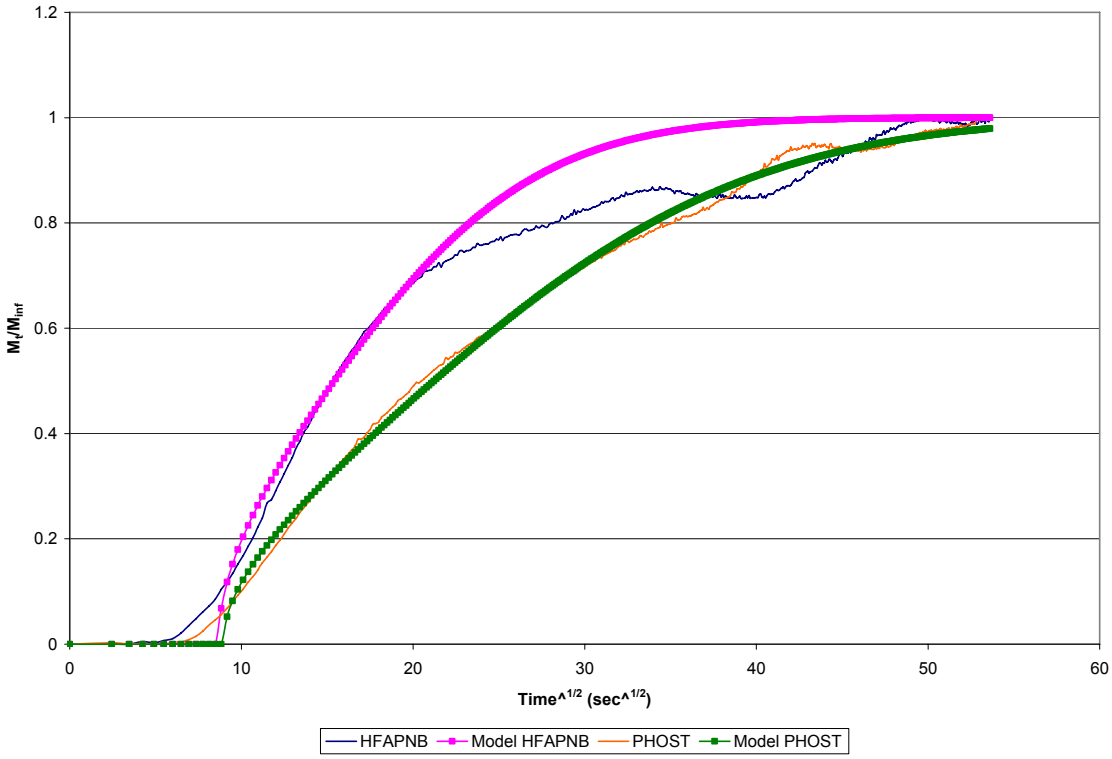

Figure 5.13: Comparison of uptake in PHOST and HFAPNB versus Theoretical Model in a 50/50 molar mixture of methanol and water.

5.1.6 Characterization of sensing layer through Refractive Index change and Thickness change.

The chemical responses of the polymer HFAPNB to the target agents water, methanol, isopropanol and benzene are measured using ellipsometry, which is enabled by a custom sealed stainless-steel chamber. From this chamber, the monitored vapor stream flows to the stainless steel test chamber, located on a high-speed, spectroscopic ellipsometer. The index and thickness of the same polymer film respond to the gas

mixture, and the changes are measured multiple times per minute. The index resolution for this measurement is approximately 1 x 10^{-4}. By utilizing this system, concentrations up to 1.4 x 10^{5} *ppmv* with a precision of ±1 *ppmv* can be delivered. This chamber allows accurate assessment of the changes of index and thickness of the sensing material in response to a range of agent concentrations. Data is acquired at a rate of ~ 0.17 *Hz*, allowing observation of the transient response of this material. The mass uptake of chemical in the sensing material, measured by the QCM, was also measured during these experiments and has been previously discussed. By measuring the mass uptake and optical constant data at one time, this provides a calibration of the various responses of the sensing layer and provides accurate physical constants for numerical simulations. To illustrate the method of data gathering from the ellipsometer, Figure 5.14 depicts the the index and thickness changes over time, of the polymer HFAPNB, in response to air saturated with methanol. This suggests that initially, methanol replaces air within the spaces in the polymer, increasing the index, shown by the sharp peak followed by a gradual fall as the methanol absorbs into the polymer. Finally, the lower-index methanol stretches the polymer, decreasing the relative amount of polymer to methanol and therefore the index. As the methanol stream is turned off and nitrogen once again flows through the system. Further support of the above hypothesis is shown as the larger thickness and smaller index is shown after the desorption of methanol. This deformation of the polymer intimately affects the sensor response.

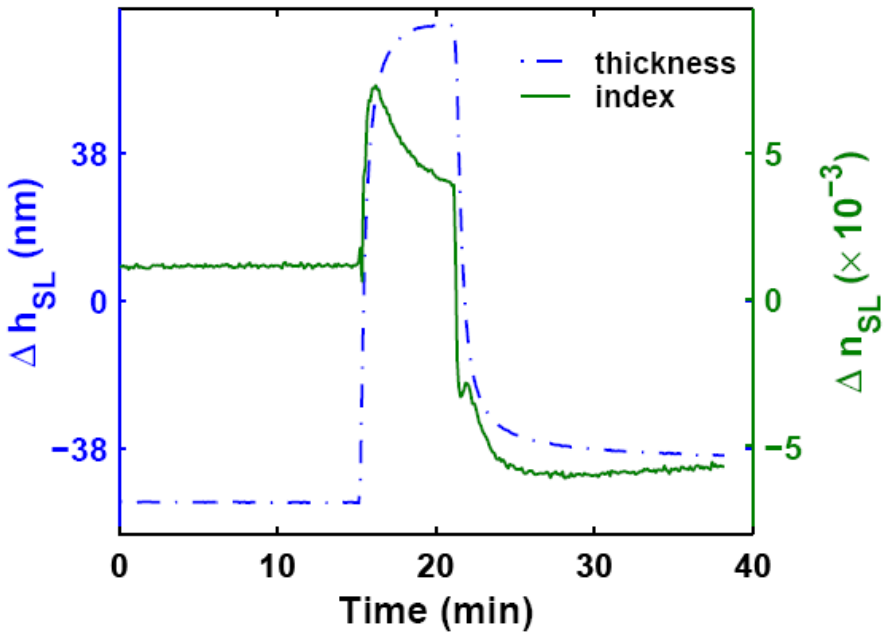

Figure 5.14: Change in index of refraction and thickness of the polymer HFAPNB in response to 71000 ppm methanol in nitrogen.

The same experiment was conducted at a lower vapor concentration of methanol, 140 *ppmv*. The change in index and thickness was then linked to the mass uptake of the polymer. This was allowed because of the link between the ellipsometer chamber and QCM and the accurate mass flow control device. Figure 5.15 depicts the index response to the 140 ppmv of methanol in Nitrogen with the corresponding QCM response, which measures mass uptake. Figure 5.16 shows the associated thickness change again with the corresponding mass uptake change from the QCM.

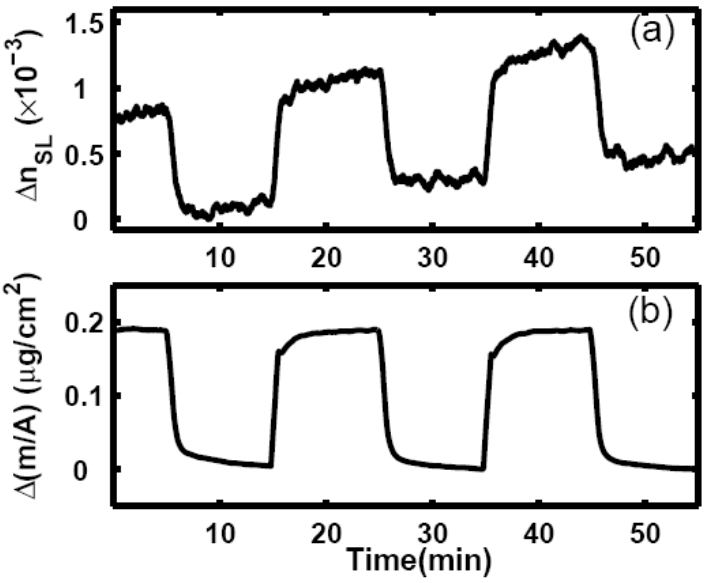

Figure 5.15: (a) Ellipsometric response of change in index of HFAPNB, to 140 *ppmv* of methanol. (b) QCM response of mass uptake, to 140 *ppmv* of methanol.

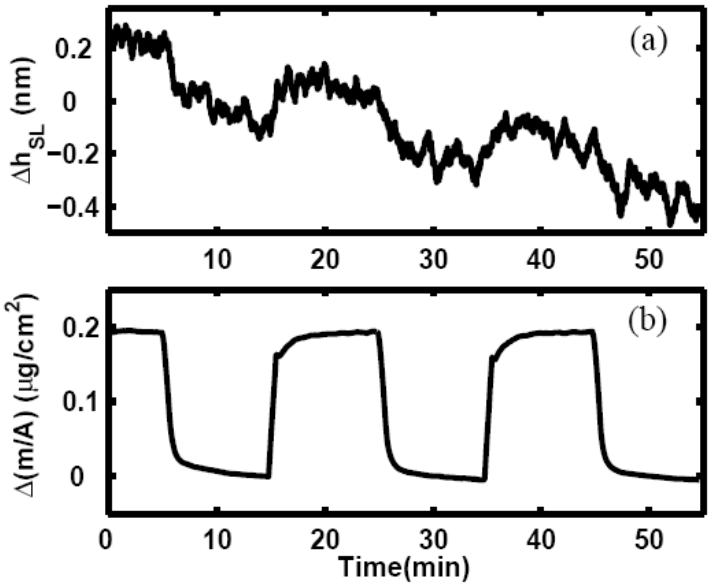

Figure 5.16: (a) Ellipsometric response, of the thickness change, Δh_{SL}, to 140 *ppmv* of methanlol. (b) QCM respons of mass uptake, to 140 *ppmv* of methanol.

Specifically, the change in the index of refraction for HFAPNB with a stream of 140ppmv of Methanol was approximately 5.4 x 10^3 [cm^2/g] and the corresponding thickness change of HFAPNB was approximately 1[$nm\ cm^2/ug$]. In addition, the mass uptake at 140 ppmv was approximately 185 [*ng/cm3*]. The thickness change is practically insignificant at this concentration change.

Again, the same experimentation was conducted except the concentration of methanol vapor is adjusted to 3, 11, 60, 120, 239, 11, and 3 *ppmv*. Figure 5.17 and Figure 5.18 shows the change in index and thickness respectively, over time. As depicted in the graphs, it seems that the real time fitting routine has produced some discontinuities in the data. By taking out these discontinues an estimate of the corrected optical response has been shown and is labeled as corrected. This corrected data is only an estimate and the overall drift in this measurement may not be characteristic of the polymer state. The changes in concentration that do not occur at the discontinuities do present true indications of changes in optical properties for the given concentration changes.

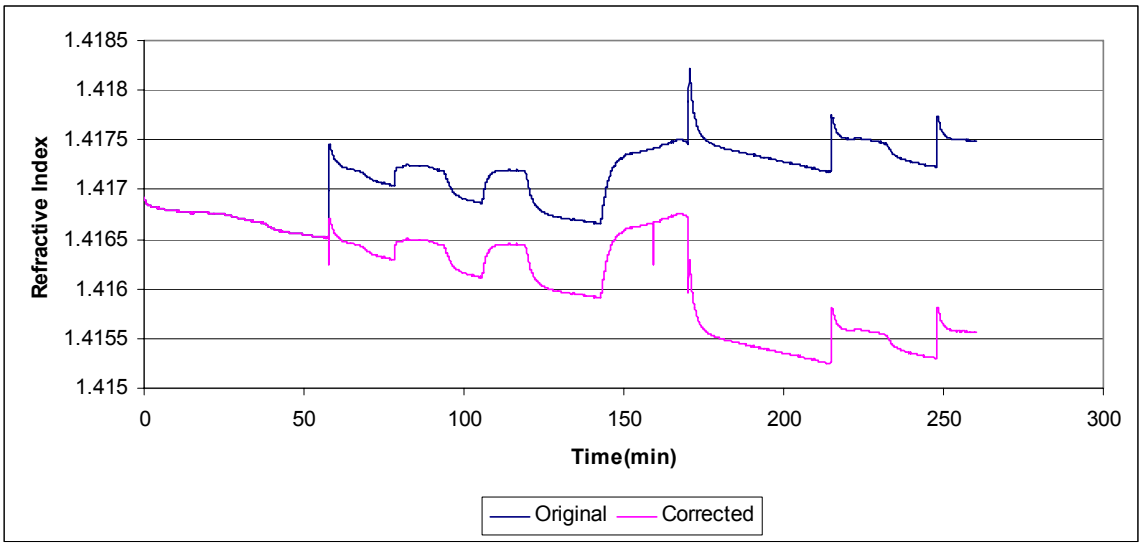

Figure 5.17: Refractive Index thickness change due to concentrations applied at 3, 11, 60, 120, 239, 11, and 3 *ppmv*.

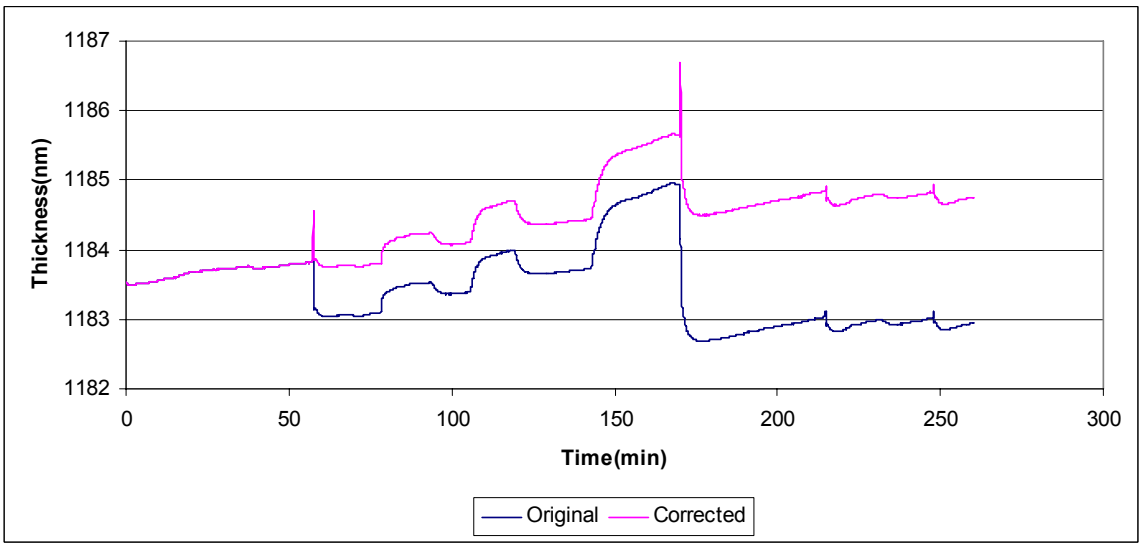

Figure 5.18: HFAPNB Thickness change due to concentrations applied at 3, 11, 60, 120, 239, 11, and 3 *ppmv*.

The index change and thickness change as a function of concentration is shown in Figure 5.19 and 5.20 respectively.

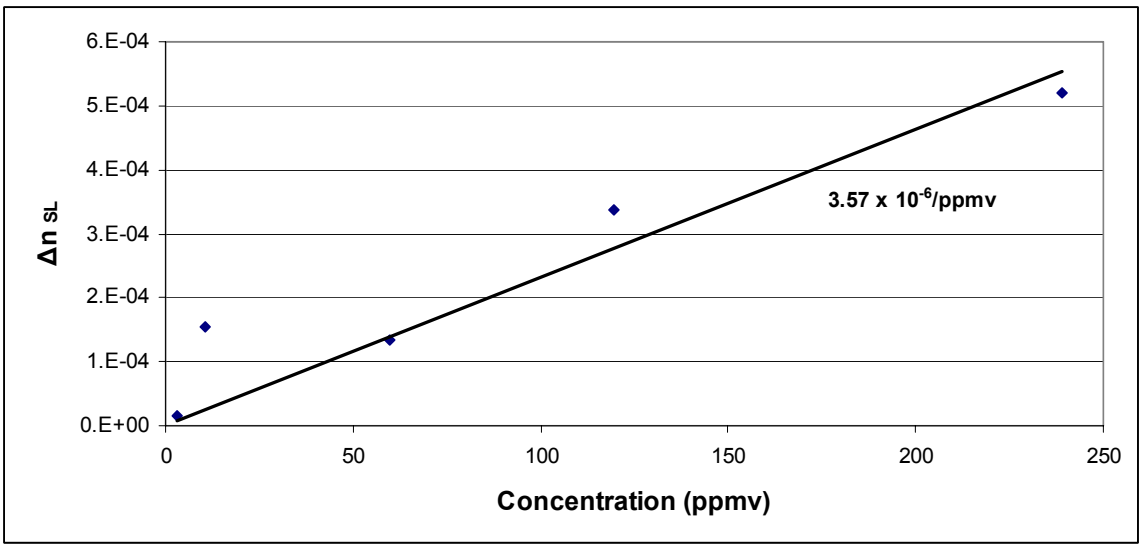

Figure 5.19: Index Sensitivity of HFAPNB to Methanol vapor concentration.

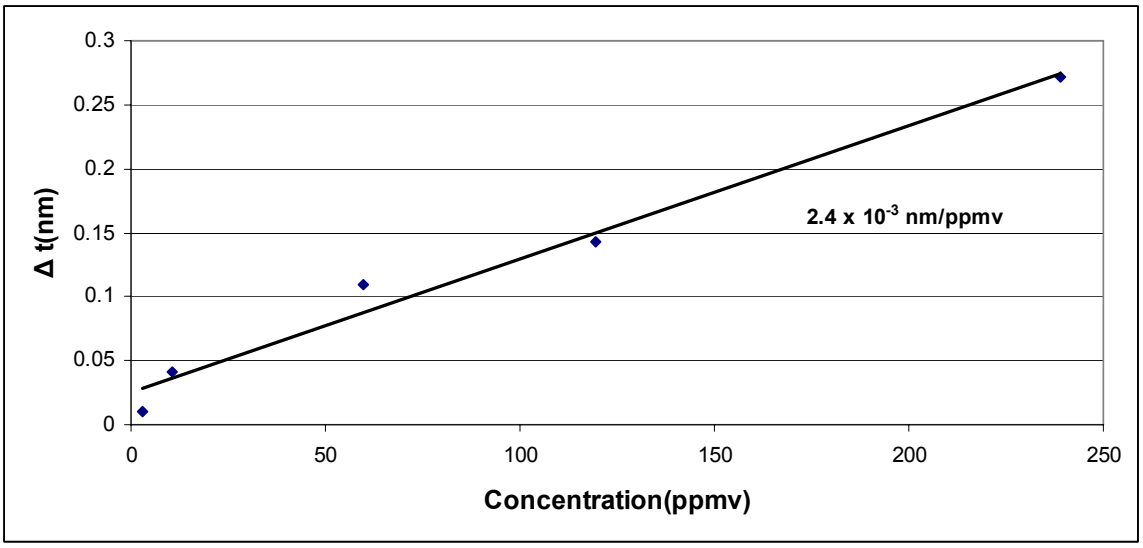

Figure 5.20: Thickness Sensitivity of HFAPNB to Methanol vapor concentration.

The gas delivery/ellipsometric chamber system permitted similar experiments to be conducted to determine the optical response of the polymer HFAPNB for other analytes including water, benzene, and isopropanol. The relationships between the concentration to the sensitivity to index and thickness change for each analyte is shown in Table 5.7

Table 5.7: The relationship of the Sensitivity of HFAPNB to different analytes with regards to refractive index and thickness of polymer.

	Δ t (nm)/ppmv	**Δn_{SL}/ppmv**
Water	4.95×10^{-4}	1.59×10^{-5}
Methanol	2.4×10^{-3}	-3.57×10^{-6}
Isopropanol	2.23×10^{-2}	-1.06×10^{-4}
Benzene	2.14×10^{-2}	5.3×10^{-5}

5.1.7 Thermal effects on the polymer HFAPNB and PHOST

Work completed by Lillie [21] has suggested that temperature changes will cause expansion or contraction related compressive or tensile stresses in layered structures. These structures include both SiO_xN_y or SiO_2 and a polymer. The stress effects between the SiO_xN_y and SiO_2 will be much smaller than that with the polymers in the structure. In general inorganic materials like SiO_2 and SiO_xN_y are far less sensitive to temperature changes than polymers. Lillie [21] has also found variation of temperature effects from different polymers such as HFAPNB and PHOST. This is why careful selection of the polymer that will be used as a sensing layer is needed. Choosing a polymer with a small sensitivity to temperature is needed for EWS's. The magnitude of the [dn/dT] determines the materials index sensitivity to temperature change. Lillie [22] has proven that both

HFAPNB and PHOST falls within reasonable bounds of the volume coefficient of thermal expansion which is 1 and 7 x 10 -4/°C.

Chapter 6

Conclusion and Future Work

In summary, this thesis has characterized the use of HFAPNB and PHOST as a sensing layer material for a fully integrated multi-mode interferometric evanescent waveguide. The compatibility of HFAPNB and PHOST with standard CMOS and MEMS processing allowed us to explore their characteristics for sensing different analytes which included water, methanol, isopropyl alcohol, and benzene. The relative sensitivity of the polymer HFAPNB and PHOST to different chemicals has been quantified and related to a refractive index shift and thickness change of the polymers. Diffusion coefficients have also been quantified for both polymers and interaction models for each polymer and analyte has been determined to predict the concentration of a mixture of analytes. Deviations from Fickian behavior could suggest the differences from the theoretical models to the experimental data. While data suggest that utilizing PHOST and HFAPNB as a sensing layer is possible, care should be taken in choosing what analyte the polymers will be quantifying. As shown in the results, it appears that as you increase the molecular weight of alcohols, the polymer starts to plasticize and loose its ability to accurately measure the amount of mass uptake or changes in optical properties. However the polymers did show more promising results when benzene was chosen as the analyte.

Despite some successes of characterizing the polymers sensing abilities, there still remain areas of future work that should be performed in order to further

refine the use of these polymers as a sensing layer material. The suggestions below should be performed in order to improve upon the sensitivity to measure different analytes.

- Understanding if purely Fickian diffusion is occurring during the uptake of the analytes or if a Case II type diffusion is occurring. Visco elastic stress can be related to the concept of a relaxation time, which measures the time it takes one portion of the polymer network to react to changes in another portion. In certain polymer-penetrant systems, this stress which is a non-linear memory effect should be taken into consideration. As shown previously there was certain deviations from Fickian Diffusion that suggested the diffusion coefficients could be dependant upon concentration. By exploring if the diffusion coefficients are dependant upon concentration this will allow a better fit of the mass uptake which will ultimately help in determining the concentration of a binary system.
- Complete more experiments of mixtures of alcohols and water to understand the relationship of the alcohol and water and determine if the analytes are competing for the same free volume. As the alcohol increased from MeOH to IPA it could be suggested that the polymer was being highly plasticized and therefore QCM measurements might not be viable. This would suggest that the polymers HFAPNB and PHOST are not sufficient to be considered

sensing layers for alcohols. Because of the similarity in the weight % uptakes for IPA and methanol with both PHOST and HFAPNB, the sensitivity of each polymer to analyte might not be significant enough to determine a difference in alcohol concentrations.

- Complete more experiments with Benzene in both HFAPNB and PHOST. With the drastic difference in wt% uptake between the two polymers it could be suggested that the viability of the polymers being a sensing layer for Benzene is an option. Expansion of similar analytes to determine the sensitivity of the polymers to encompass a broader range of contaminants for detection is also suggested.

Appendix A

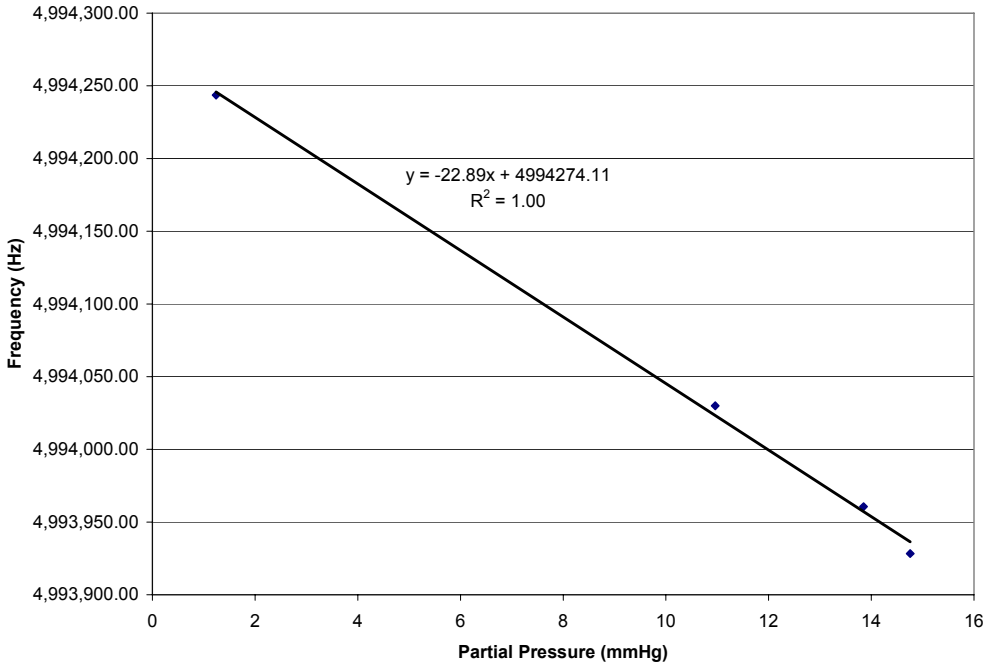

Figure A.1: Linear relationship between QCM crystal frequency for PHOST and water partial pressure.

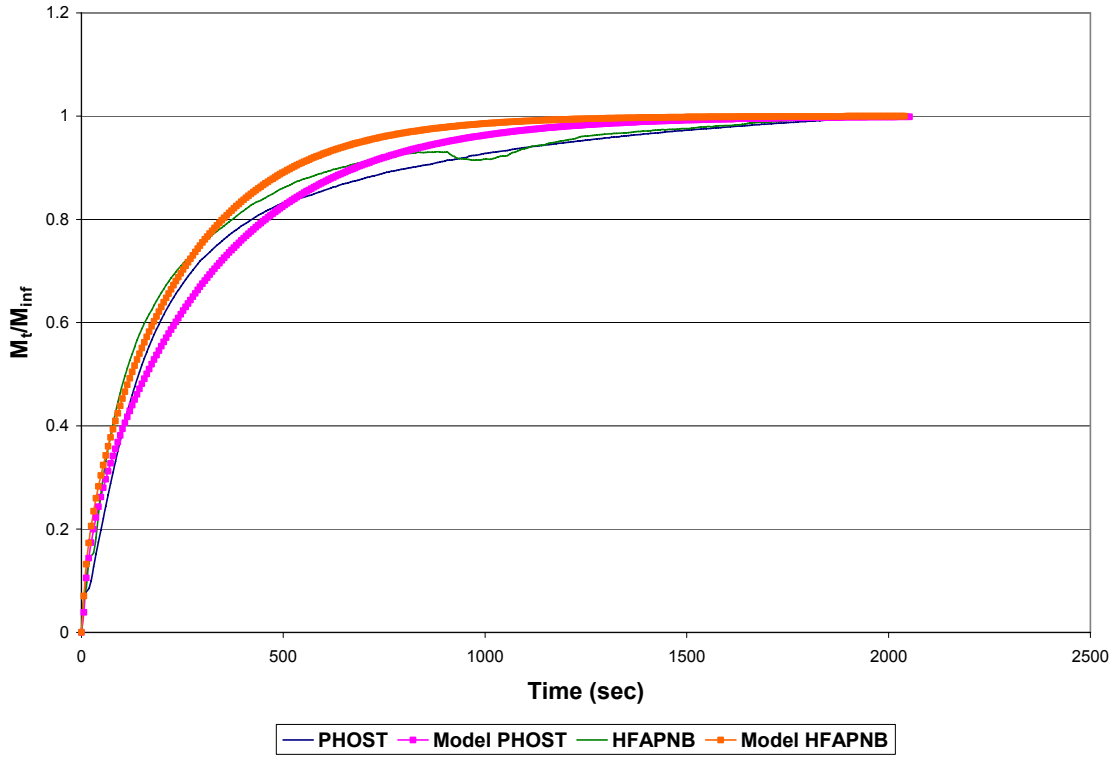

Figure A.2: Comparison of uptake of water in PHOST and HFAPNB versus Theoretical Model.

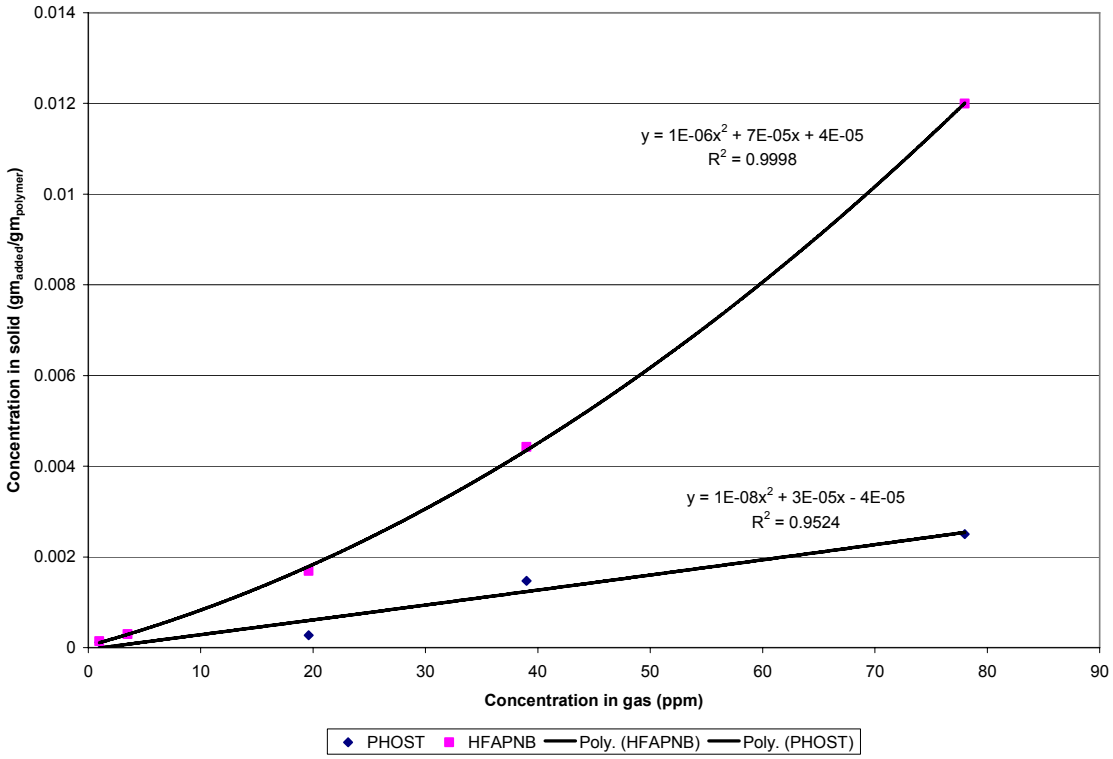

Figure A.3: Interaction Model for PHOST and HFAPNB of IPA

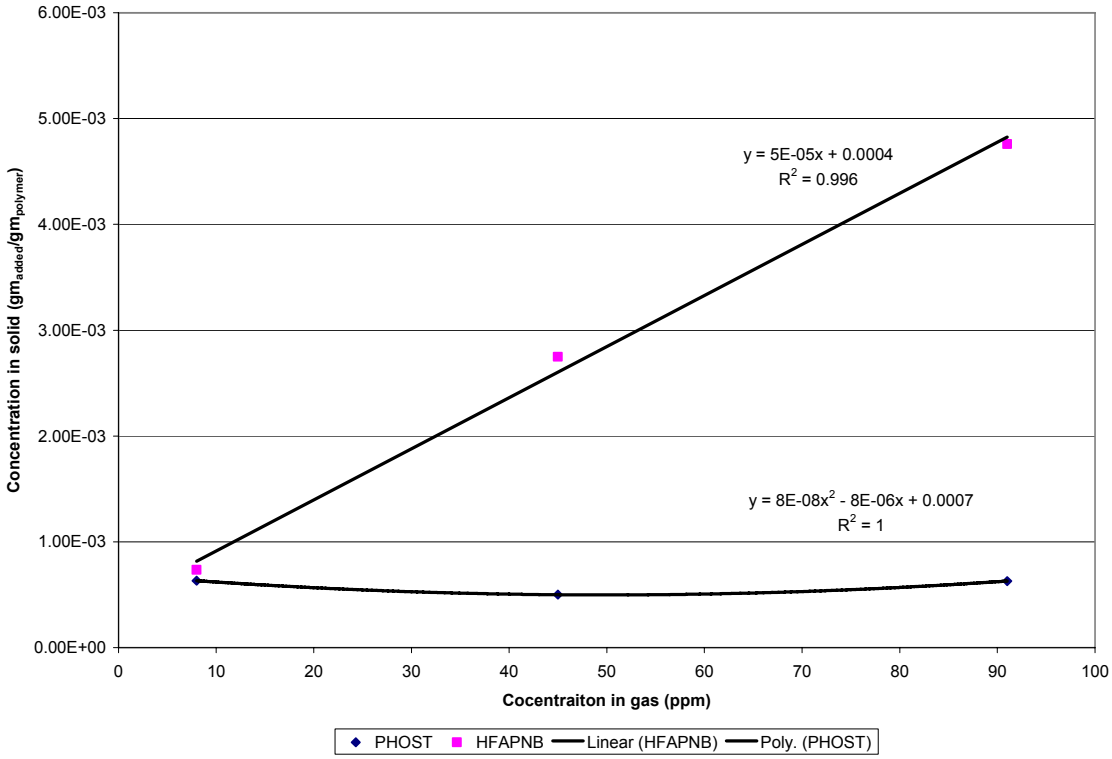

Figure A.4: Interaction Model for PHOST and HFAPNB of Benzene

MatLab Code

```
function fd_model1

%Models the absorption of analyte

thickness = 0.001153; %thickness of sample
time = 996; %length of time for simulation
ni = 43; % number of spatial nodes because there is a node at i=1, ... , n
nt = 20000; % number of time points because time = 1, ...., n
dx = thickness/(ni-1) ; %node spacing
dt = time/(nt-1); % time increments
D = 0.000000007307; %diffusion coefficient
tau=26; %residence time
Cnom = 68000; %concentration
Cfinal=4E-06*Cnom+0.0025

c(ni,nt)=zeros;

Cgas = Cnom*(1-exp(-dt/tau)); %Concentration in gas ppm
Csolid = 4E-06*Cgas+0.0025; %Nonlinear concentration model
currentime(1)=0

MtMinf(1)=0

for i=1:ni;
   location(i)=dx*(i-1);
end

c(ni,1)=Csolid;
%for i=1:ni-1;
%    c(i,1)=0;
%end

for j = 2:nt;
   currenttime(j)=dt*(j-1);
   Cgas = Cnom*(1-exp(-currenttime(j)/tau)); %Concentration in gas ppm
   Csolid = 4E-06*Cgas+0.0025 %Nonlinear concentration model
   c(ni,j) = Csolid;
   % c(ni-1,j+1) = c(ni-1,j) +((D*dt)/(dx)^2)*(Csolid-2*c(ni-1,j)+c(ni-2,j));
   c(1,j) = c(1,j-1) + ((D*dt)/(dx)^2)*(c(2,j-1)-c(1,j-1));
   for i = 2:ni-1;
      c(i,j) = c(i,j-1) +((D*dt)/(dx)^2)*(c(i+1,j-1)-2*c(i,j-1)+c(i-1,j-1));
   end
   MtMinf(j)=mean(c(:,j))/Cfinal;
end
```

```
%for j=1:(nt/10):nt;
%    plot(location(:,j),c(:,j));
%end

%plot(currenttime(:),c(40,:))

%plot
(location(:),c(:,1),location(:),c(:,round(nt/5)),location(:),c(:,round(2*nt/5)),location(:),c(:,r
ound(3*nt/5)),location(:),c(:,round(4*nt/5)),location(:),c(:,nt))

plot(currenttime(:),MtMinf(:))

datatowrite=[currenttime(:),MtMinf(:)]
xlswrite('tempdata.xls', datatowrite, 'MtMinfvsTime', 'A1');


end
```

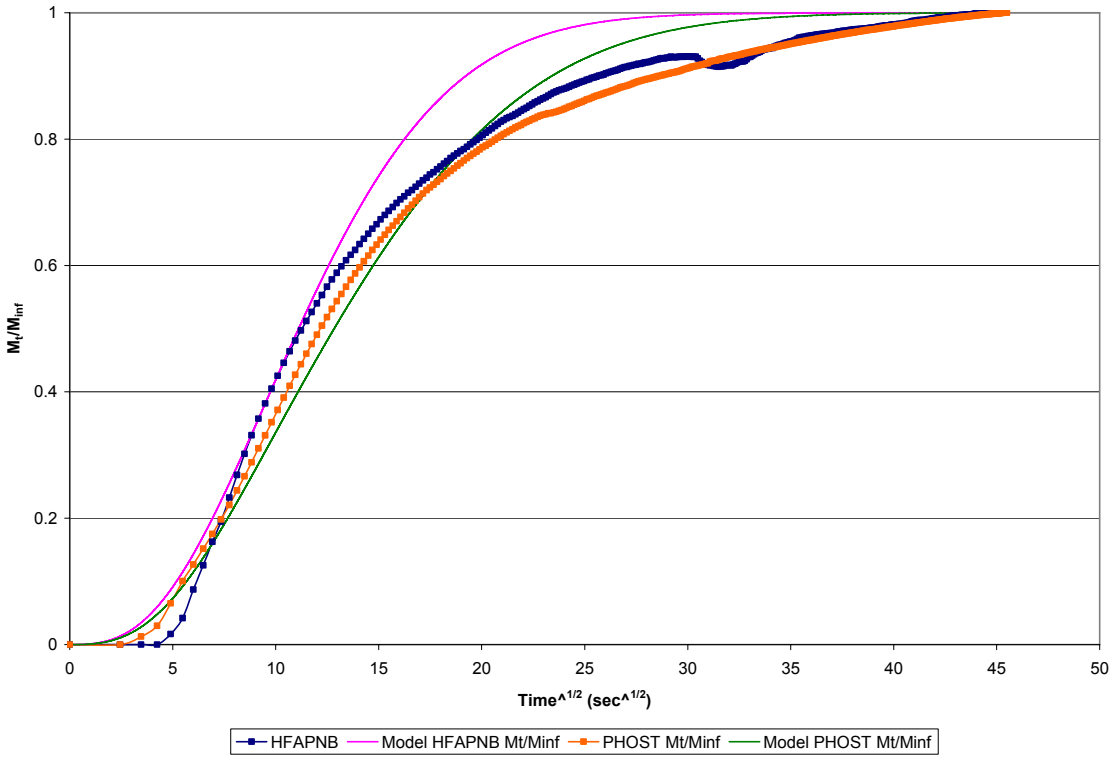

Figure A.5: Comparison of experimental data and CSTR model for Water in both PHOST and HFAPNB

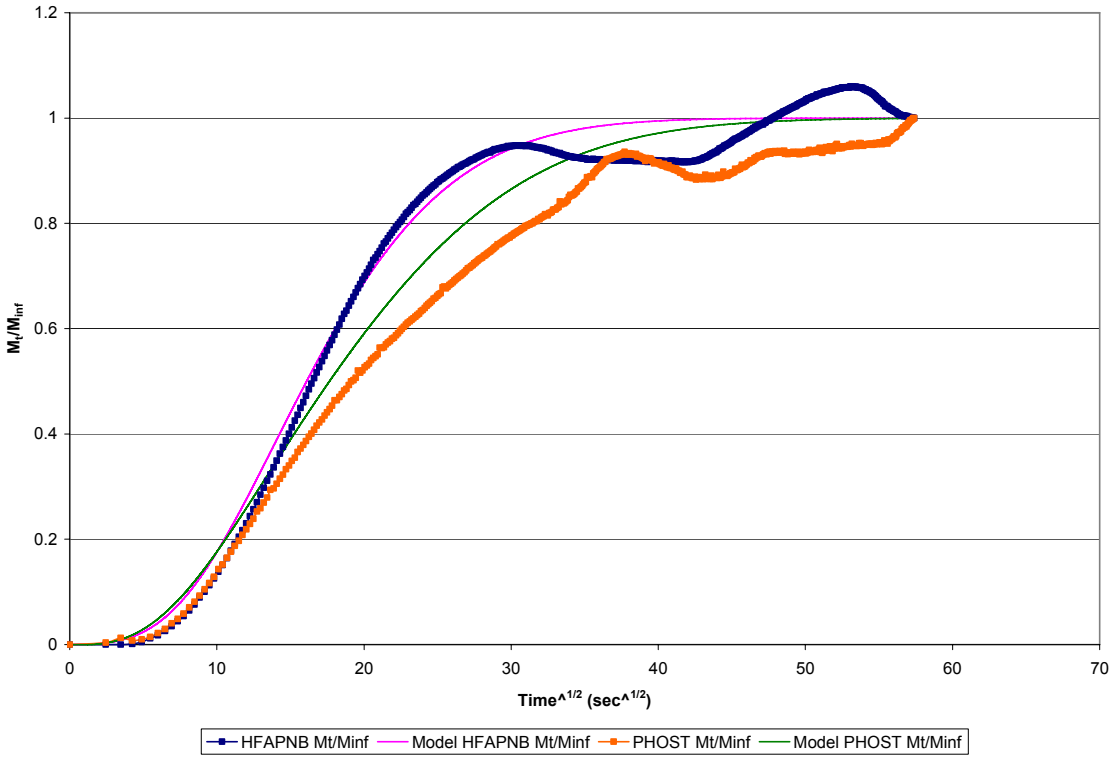

Figure A.6: Comparison of experimental data and CSTR model for IPA in both PHOST and HFAPNB

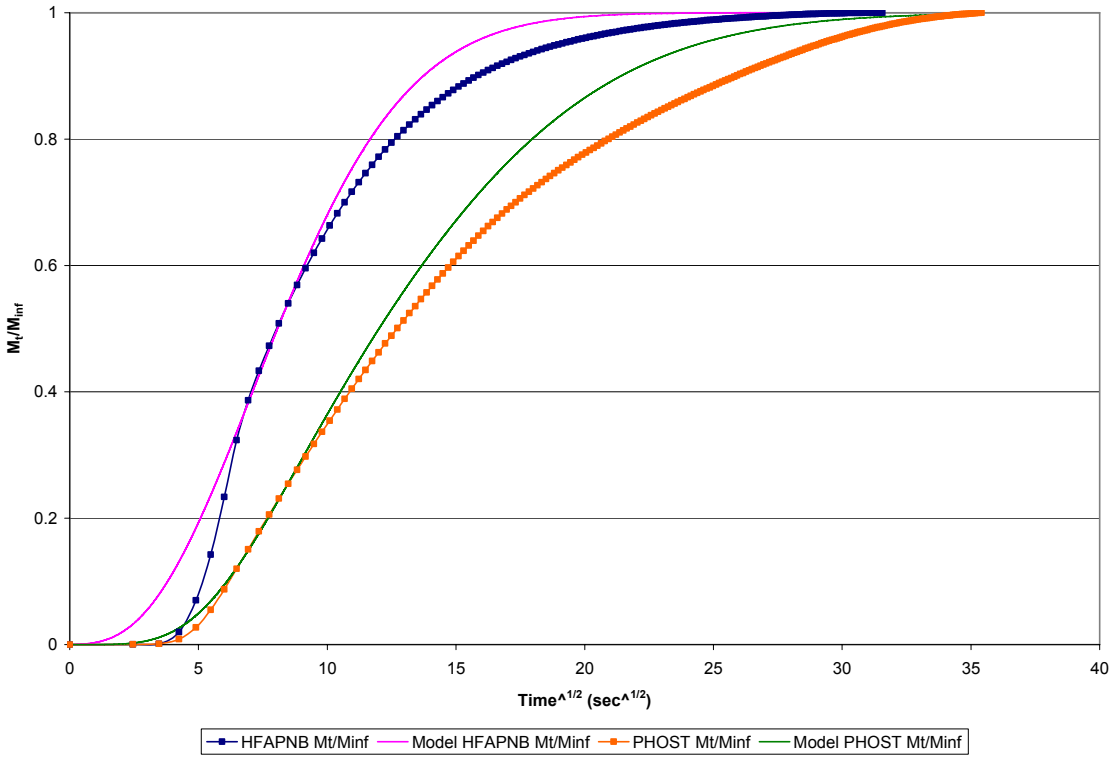

Figure A.7: Comparison of experimental data and CSTR model for Benzene in both PHOST and HFAPNB

References

1. Cattrall, R.W., *Chemical Sensors*. Vol. 52. 1997, Oxford: Oxford University Press. 74.

2. Eggins, B.R., *Chemical Sensors and Biosensors*. Analytical Techniques in the Sciences. 2002, New York: John Wiley. 273.

3. Deakin, M.R. and D.A. Buttry, *Electrochemical applications of the quartz crystal microbalance.* Analytical Chemistry, 1989. **61**(20): p. 1147A-1148A, 1150A-1154A.

4. Janshoff, A., H.-J. Galla, and C. Steinem, *Piezoelectric mass-sensing devices as biosensors-an alternative to optical biosensors?* Angewandte Chemie, International Edition, 2000. **39**(22): p. 4004-4032.

5. Boisde, G. and A. Harmer, *Chemical and Biochemical Sensing with Optical Fibers and Waveguides*. 1996, Boston: Artech House. 389.

6. Lukosz, W., *Integrated optical chemical and direct biochemical sensors.* Sensors and Actuators, B: Chemical, 1995. **B29**(1-3): p. 37-50.

7. Wolfbeis, O.S., *Fiber-Optic Chemical Sensors and Biosensors.* Analytical Chemistry, 2004. **76**(12): p. 3269-3284.

8. Schipper, E.F., et al., *The Waveguide Mach-Zender Interferometer as Atrazine Sensor.* Analytical Chemistry, 1998. **70**(6): p. 1192-1197.

9. Sarkisov, S.S., et al., *Single-arm double-mode double-order planar waveguide interferometric sensor.* Applied Optics, 2001. **40**(3): p. 349-359.

10. Qi, Z.-m., et al., *A design for improving the sensitivity of a Mach-Zehnder interferometer to chemical and biological measurands.* Sensors and Actuators, B: Chemical, 2002. **B81**(2-3): p. 254-258.

11. Hua, P., et al., *Integrated optical dual Mach-Zehnder interferometer sensor.* Sensors and Actuators, B: Chemical, 2002. **B87**(2): p. 250-257.

12. Busse, S., et al., *Gold and thiol surface functionalized integrated optical Mach-Zehnder interferometer for sensing purposes.* Sensors and Actuators, B: Chemical, 1999. **B60**(2-3): p. 148-154.

13. Zappe, H.P., *Semiconductor optical sensors.* Sensors Update, 1999. **5**: p. 3-44.

14. Janata, J., et al., *Chemical Sensors.* Analytical Chemistry, 1998. **70**(12): p. 179R-208R.

15. Hartman, N.F., J. Cobb, and J.G. Edwards, *Optical system-on-a-chip for chemical and biochemical sensing: the platform.* Proceedings of SPIE-The International Society for Optical Engineering, 1999. **3537**(Electro-Optic, Integrated Optic, and Electronic Technologies for Online Chemical Process Monitoring): p. 302-309.

16. Campbell, D.P., et al., *Reversible integrated optic evanescent field biosensor using chemical amplification for added sensitivity.* Proceedings of SPIE-The International Society for Optical Engineering, 1998. **3253**(Biomedical Sensing and Imaging Technologies): p. 20-26.

17. Campbell, D.P., et al., *Polymers: The key ingredient in waveguide chemical sensors.* Book of Abstracts, 216th ACS National Meeting, Boston, August 23-27, 1998: p. POLY-576.

18. Adhikari, B. and S. Majumdar, *Polymers in sensor applications.* Progress in Polymer Science, 2004. **29**(7): p. 699-766.

19. Akmal, N. and A.M. Usmani, *Polymers in Sensors: Theory and Practice*. ACS Symposium Series. Vol. 690. 1998, Washington, DC: American Chemical Society. 302.

20. Bader, M.A., H.M. Keller, and G. Marowski, *Polymer-based waveguides and optical switching.* Optical Materials (Amsterdam), 1998. **9**(1-4): p. 334-341.

21. Lillie, Jeffery, et al., *A Highly Sensitive, Integrable, Multimode, Interferometric Evanescent-Wave Chem/bio Sensor*. PHD Defense Dissertation Georgia Tech

22. Lillie, Jeffery, et al, *Multimode interferometric sensors on silicon optizmized for fully integrated complementary-metal-oxide-semiconductor chemical-biological sensor systems*. J. Opt. Soc. Am Vol. 23. 2006